Zoological Journal of the Linnean Society, 2018, **XX**, 1–32. With 11 figures.

Anatomy and phylogeny of the large shark-toothed dolphin *Phoberodon arctirostris* Cabrera, 1926 (Cetacea: Odontoceti) from the early Miocene of Patagonia (Argentina)

MARIANA VIGLINO[1]*, MÓNICA R. BUONO[1], R. EWAN FORDYCE[2], JOSÉ I. CUITIÑO[1] and ERICH M. G. FITZGERALD[3]

[1]*Instituto Patagónico de Geología y Paleontología, CCT CONICET-CENPAT, Puerto Madryn, Chubut, Argentina*
[2]*Department of Geology, University of Otago, Dunedin, New Zealand*
[3]*Museums Victoria, Melbourne, Victoria, Australia*

Received 12 March 2018; revised 1 June 2018; accepted for publication 20 June 2018

The early Miocene of Patagonia (Argentina) provides one of the best-known records of odontocetes for an age interval with scarce fossils. Most of these taxa are historically old and briefly described, which has contributed, in part, to their controversial taxonomic position. The shark-toothed dolphin *Phoberodon arctirostris* was described almost 100 years ago and suggested as a member of Platanistoidea and Squalodontidae. However, it has not been analysed recently and has never been included in a phylogenetic analysis. Recent fieldwork in the early Miocene sediments in Patagonia yielded a new specimen referred to this species, allowing for its modern and detailed description and the first phylogenetic analyses. Analyses recovered *P. arctirostris* as a stem Odontoceti or an early-diverging platanistoid, more closely related to an unnamed Oligocene specimen from New Zealand and not in a clade with *Squalodon calvertensis* (i.e. Squalodontidae). The reconstructed body length of *P. arctirostris* indicates that it is one of the largest stem Odontoceti. Our results suggest that during the early Miocene of Patagonia, archaic odontocete forms (i.e. *P. arctirostris*) cohabited with archaic and more crownward platanistoids (i.e. *Aondelphis talen* and *Notocetus vanbenedeni*), helping to characterize the early Miocene cetacean communities of Patagonia.

ADDITIONAL KEYWORDS: Chubut province – dolphin – Gaiman Formation – Odontoceti – Platanistoidea – Squalodontidae – stratigraphy.

INTRODUCTION

The Oligocene–early Miocene is a crucial time in the evolutionary history of odontocetes, marked by the diversification of archaic forms and the origin of modern groups (Fordyce & Muizon, 2001). However, there is an important early Miocene gap in the fossil record of odontocetes, when fossils are globally scarce. Fossil toothed cetaceans from Patagonia (early Miocene, Gaiman Formation, Argentina) provide one of the best-known records of odontocetes for the early Miocene, with representatives of platanistoids, physeteroids, eurhinodelphinids and kentriodontids (e.g. Lydekker, 1894; Cozzuol, 1996; Buono *et al.*, 2016; Viglino *et al.*, 2018). In particular, Platanistoidea (a clade that includes Oligocene–Miocene disparate forms but only one extant genus, *Platanista*) is the most diverse group recorded in the early Miocene beds of Chubut province (Patagonia), including *Prosqualodon australis* Lydekker, 1894, *Phoberodon arctirostris* Cabrera, 1926 and *Notocetus vanbenedeni* Moreno, 1892 (e.g. Moreno, 1892; Lydekker, 1894; Cabrera, 1926; Cozzuol, 1996; Cione *et al.*, 2011). Most of these Patagonian taxa were briefly described and illustrated in the 19th century, based on single incomplete specimens. The lack of detailed modern descriptions for these and other key taxa has contributed to the controversy over the contents of Platanistoidea. Some recent revisions of Oligocene taxa shed light on the early diversity of platanistoids during this time and offer new phylogenetic hypotheses

*Corresponding author. E-mail: viglino@cenpat-conicet.gob.ar

(e.g. Tanaka & Fordyce, 2014, 2015a,b, 2016, 2017; Boersma & Pyenson, 2016). However, the phylogenetic position of some taxa (e.g. *Squalodon*, *Prosqualodon*) and even the contents of Platanistoidea remain unclear (e.g. Lambert *et al.*, 2014; Tanaka & Fordyce, 2014, 2015a,b, 2016, 2017; Boersma & Pyenson, 2016; Boersma *et al.*, 2017; Viglino *et al.*, 2018).

The Patagonian shark-toothed dolphin *P. arctirostris* was originally described by Cabrera (1926) based on two well-preserved skeletons from the early Miocene of Patagonia. Despite its early description, *P. arctirostris* has not been documented or analysed in detail and has never been included in a phylogenetic analysis. The original description is brief, lacking descriptions or figures for some key regions of the skull (e.g. the basicranium). Neither the holotype nor MLP 5-3 specimens have the tympanoperiotic preserved. Cabrera (1926) originally identified this taxon within Squalodontidae, an interpretation that was later supported by Simpson (1945) and Fordyce (1994) but without a phylogenetic analysis. Cozzuol (1996) made some comments on the basicranium of the holotype and discussed its relationships briefly, suggesting a close relationship with *Waipatia maerewhenua* Fordyce, 1994, but did not perform a phylogenetic analysis. Muizon (1987, 1991, 1994) commented on the morphology of the scapula and squamosal and suggested that *P. arctirostris* belongs within Platanistoidea. Kimura *et al.* (2009) and Fitzgerald (2016) made only a brief mention on the scapular morphology of *P. arctirostris*.

As a result of recent fieldwork in the early Miocene sediments of Chubut province (Magagna Beach; Gaiman Formation) in Patagonia, a new specimen referred to this species was collected, including well-preserved and informative elements of the postcranial skeleton (notably, both scapulae). The goal of this paper is to redescribe and rediagnose *P. arctirostris* based on the previously known materials of Cabrera and on the new specimen. A phylogenetic analysis including this species is presented.

MATERIAL AND METHODS

Institutional abbreviations

AMNH, American Museum of Natural History, New York, NY, USA; MLP, Museo de La Plata, La Plata, Argentina; MPEF-PV, Museo Paleontológico 'Egidio Feruglio', Trelew, Argentina; NMNS, National Museum of Natural Science, Taichung city, Taiwan; OU, Geology Museum, University of Otago, Dunedin, New Zealand; TMAG, Tasmanian Museum and Art Gallery, Hobart, Tasmania, Australia; USNM, Department of Paleobiology and Department of Vertebrate Zoology, National Museum of Natural History, Smithsonian Institution, Washington, DC, USA; ZMT, Fossil mammals catalogue, Canterbury Museum, Christchurch, New Zealand. These institutions are accessible, permanent repositories.

Materials and terminology

The redescription of *P. arctirostris* is based on the holotype (MLP 5-4) and MLP 5-3, deposited at the División Paleontología de Vertebrados in Museo La Plata in La Plata, Buenos Aires province, Argentina. The holotype was collected in August 1899, and MLP 5-3 was collected by Cremonessi in 1895; both specimens were collected from Cerro Castillo, close to Trelew, Chubut province (Cabrera, 1926). Also, a new referred specimen was included (MPEF-PV 10883), deposited at the Museo Paleontológico 'Egidio Feruglio' in Trelew, Chubut province, Argentina. Data from the literature and specimens held in scientific collections were used in the comparative and phylogenetic studies (see Supporting Information, Appendix S1).

Descriptions are based on the right or left side, whichever is more informative, with differences between them mentioned only if directional asymmetry is evident. For the skull, morphological terms follow Mead & Fordyce (2009), and postcranial terms follow Rommel (1990) and Rommel & Reynolds (2008), unless otherwise noted. For identification of muscle attachments of the humerus, we followed Howell (1930), Schulte & Smith (1918), Smith *et al.* (1976), Strickler (1978) and Gutstein *et al.* (2014).

Preparation of the specimens

The several large portions of the skull and mandible of the holotype are cradled in a metal wire-and-strapping support, which introduces some measuring errors. The newer MPEF-PV 10883 was prepared using pneumatic chisels and hand tools, with finishing carried out under a Zeiss SR binocular microscope at ×8 or ×12 magnification, by Santiago Bessone at Instituto Patagónico de Geología y Paleontología (IPGP-CENPAT). It was glued with cyanoacrylate and coated with Butvar B-76 consolidant. This new specimen was recovered in ~3 h, as dictated by the intertidal setting. Photographs were taken either with a Nikon D800 DSLR camera with a 105 mm micro lens and D3000 with a 16–35 mm lens, Canon Powershot G16 or an Olympus E-M1. An image-stacking technique (Bercovici *et al.*, 2009) was used to obtain a well-focused image, by merging several images captured at slightly different focal planes. Finally, each resulting stacked image was checked for artefacts.

Phylogenetic analyses

The starting point for the phylogenetic analysis was the matrix published by Tanaka & Fordyce (2016) without

the backbone constraint, and it was managed using Mesquite v. 2.75 (Maddison & Maddison, 2011). The original matrix was expanded by adding three taxa, as follows: *P. arctirostris*, an undescribed squalodontid species represented by OU 21798, and the codings for the recently published *Inticetus vertizi* Lambert *et al.*, 2018 (Lambert *et al.*, 2018). The list of character and coding modifications made for the present study are listed in the Supporting Information (Appendix S2). Thus, the resulting matrix has 86 taxa and 285 characters (226 craniomandibular, 28 postcranial and 31 soft-tissue characters). *Phoberodon arctirostris* has 48% missing data, including the character-rich tympanoperiotics, and OU 21798 has 29% missing data (both including soft-tissue characters; see Supporting Information, Appendix S3 for full matrix).

Heuristic parsimony analysis of the data set was performed in TNT v. 1.5 (Goloboff & Catalano, 2016) under equal and implied weights (concavity value, K = 1–33). All characters were treated as unordered. The analysis was performed using 1000 replicates of Wagner trees (using random addition sequences), tree bisection reconnection (TBR) branch swapping, and holding 10 trees per replicate. The best trees obtained at the end of the replicates were subjected to a final round of TBR branch swapping. The resulting most parsimonious trees (MPTs) were summarized using strict consensus trees with zero-length branches collapsed (i.e. 'rule 1' of Coddington & Scharff, 1994). For branch support, jackknife resampling analysis (using probability, P = 0.30 and 1000 pseudoreplicates) and Bremer support were performed. To identify unstable taxa, we applied the IterPCR procedure (Pol & Escapa, 2009; Escapa & Pol, 2011) over the entire set of MPTs.

After the analyses, as above, species in the more diverse clades crownward of *Papahu*, *Squaloziphius* and *Xiphiacetus* were merged for ease of illustration. The full cladograms, which show positions for all operational taxonomic units, are provided in the Supporting Information (Appendix S4).

Geological setting

The specimens described here were collected from sediments of the Gaiman Formation (Mendía & Bayarsky, 1981) at El Castillo and Playa Magagna localities (Fig. 1A, B). The Gaiman Formation consists of a succession of mudstones, fine tuffs, sandstones, tuffaceous sandstones and sparse shell beds, deposited in marine environments that graded from the inner shelf to the shoreline (Scasso & Castro, 1999). In the discussion below, international stages (e.g. Burdigalian) are used where there is sufficient resolution; otherwise, the ages are cited as undifferentiated sub-epochs (e.g. early Miocene).

Cerro Castillo is located ~10 km south of Trelew city, in the southern margin of the Lower Valley of the Chubut River, Chubut province (Fig. 1A, B). Along the southern margin of this valley, a 200-m-thick, subhorizontal sedimentary succession is exposed, comprising Palaeogene–Neogene continental and marine units (Fig. 1C; Scasso & Castro, 1999; Scasso & Bellosi, 2004), including the Gaiman Formation. The latter is nearly 100 m-thick in Cerro Castillo (Fig. 1C) and unconformably overlies the Trelew Member of the Sarmiento Formation (early Miocene), composed of yellowish to whitish-grey, sandy tuffs and tuffs with continental mammals (Simpson, 1935; Fleagle & Bown, 1983; Scasso & Bellosi, 2004). In turn, the Gaiman Formation is unconformably overlain by a 30-m-thick succession of cross-bedded sandstones and heterolithic deposits referred as the Puerto Madryn Formation (Fig. 1C), accumulated in estuarine environments (Scasso & Castro, 1999). At Cerro Castillo, most of the cetacean remains come from the lower half of the Gaiman Formation (Buono *et al.*, 2017), which is composed of thoroughly bioturbated siltstones and fine sandstones, with articulated oysters and other molluscs. This evidence, plus the intercalated storm deposits, suggest deposition in an inner shelf environment.

Playa Magagna locality lies ~20 km east of Cerro Castillo and 5 km south of Playa Unión (Fig. 1B). There, the stratigraphic section composes nearly 10 m of the Gaiman Formation, which is unconformably covered by Quaternary coarse-grained fluvial sediments. Outcrops of the Gaiman Formation lie mostly in the wave-cut platform (*restinga* in Spanish), where specimen MPEF-PV 10883 was collected, and are exposed during low tide. Additionally, part of the exposures composed the associated small coastal cliffs. In this locality, the unit is composed of thoroughly bioturbated fine sandstones and mudstones, also with articulated oysters and other molluscs, which suggests an inner shelf marine environment.

A thicker succession of the Gaiman Formation crops out ~15 km south of Playa Magagna. The base of the unit is not exposed. Here, Acosta Hospitaleche *et al.* (2008) described a stratigraphic section of ~100 m, referring the levels of the wave-cut platform of Playa Magagna to the lower third of the unit. This means that the Playa Magagna levels, where specimen MPEF-PV 10883 was extracted, correlate with the lower third of the Gaiman Formation of Cerro Castillo (Fig. 1C).

The age of the Gaiman Formation is based on stratigraphic correlations with other, better-dated sections in Patagonia and biostratigraphic data. The 'Patagoniense' marine deposits, equivalent to the Gaiman Formation, were dated in the Austral Basin (Santa Cruz Province, Patagonia) by means of U–Pb dating of zircon grains and Sr–Sr dating of oyster valves, with results in the range 20.05–15.37 Mya, indicating early Miocene (Cuitiño *et al.*, 2012, 2015a; Parras *et al.*, 2012). Equivalent beds in the Comodoro Rivadavia region

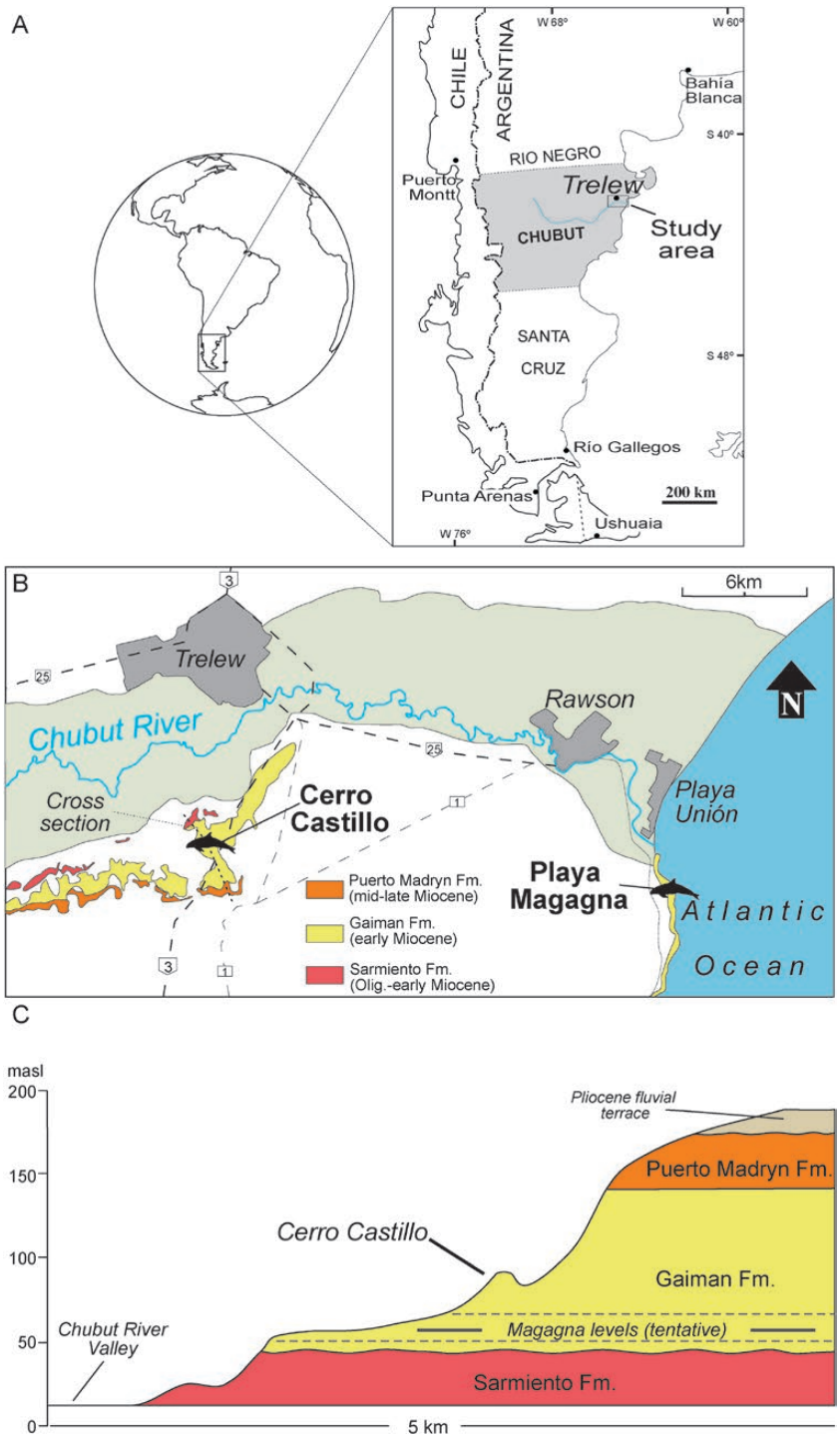

Figure 1. Map and stratigraphic section of the geographical and stratigraphic occurrence of *Phoberodon arctirostris*. A, regional map of the study area. B, detailed map with stratigraphic information of the type locality of MLP 5-4 and MLP 5-3 (Cerro Castillo), and locality of MPEF-PV 10883 (Playa Magagna) indicated by dolphin outline. Only the Neogene outcrops of the southern margin of the Chubut river valley are mapped. C, simplified stratigraphic section of the Neogene outcrops of the southern margin of the Chubut river valley. The location of the section is indicated in (B).

(Chubut province), dated by the Sr–Sr method, comprise a longer depositional age, spanning from the early Miocene (Burdigalian) to the middle Miocene (early Langhian; Cuitiño *et al.*, 2015b). The initial flooding phase of the Patagoniense transgression occurred in the Aquitanian to early Burdigalian (e.g. Cuitiño *et al.*, 2015b), whereas the younger deposits of the regressive interval extend only locally to the Langhian age (Cuitiño *et al.*, 2015b). The lower beds of the Gaiman Formation assessed here represent the initial phase of the 'Patagoniense' marine cycle. Based on regional correlations, an early Miocene age of unresolved international stage is proposed for these cetacean-bearing beds. This age is also suggested by the Colhuehuapian mammal fauna recovered from the underlying Trelew Member of the Sarmiento Formation (Flynn & Swisher, 1995; Dunn *et al.*, 2013). In addition, evidence from marine vertebrates in the Gaiman Formation (i.e. fishes and penguins; Cione *et al.*, 2011) and a palynological assemblage recovered from the study area (Palazzesi *et al.*, 2006) also indicate an early Miocene age.

RESULTS

SYSTEMATIC PALEONTOLOGY

CETACEA BRISSON, 1762

ODONTOCETI FLOWER, 1867

PHOBERODON CABRERA, 1926

Type and only known species: *Phoberodon arctirostris* Cabrera, 1926.

Emended diagnosis of genus: As for the type and only species known.

PHOBERODON ARCTIROSTRIS CABRERA, 1926

(FIGS 2–10; TABLES 1–3)

Holotype: MLP 5-4: incomplete skull (including maxillae, premaxillae, palatines, nasals, ethmoid, vomer, frontals, a small portion of the supraoccipital and exoccipitals, squamosals and a small portion of the sphenoids), almost complete mandibles, 35 vertebrae (five cervical, eight thoracic, 12 lumbar and ten caudal), four chevrons, ribs, incomplete right scapula and right humerus and radius. Cabrera (1926) figured the lacrimojugals, but both are now lost.

Referred specimens: MLP 5-3: nearly complete skull (including most of the maxillae and premaxillae, palatines, nasals, ethmoid, vomer, frontals, a portion of the supraoccipital and exoccipitals, squamosals, part of the pterygoid and sphenoids), incomplete mandible, 34 vertebrae (four cervical, ten thoracic, 11 lumbar and ten caudal), one chevron, ribs and manubrium. Cabrera (1926) mentioned 36 vertebrae for this specimen, but only 34 could be located.

MPEF-PV 10883: incomplete skull (including maxillae, premaxillae, nasals, frontals, ethmoid, a portion of right lacrimojugal, a portion of the vomer and right orbitsphenoid and a small portion of the supraoccipital), incomplete left mandible, 15 vertebrae (three cervical, six thoracic, four lumbar and two caudal), ribs, a right humerus and both incomplete scapulae. The skull presents a little diagenetic deformation on the rostrum and to a lesser degree in the cranium.

Geographical and stratigraphic occurrence: The holotype and MLP 5-3 specimens are from Cerro Castillo (43°20′12.3″S, 65°19′10.7″W), to the south of Trelew city, whereas MPEF-PV 10883 was collected on Magagna beach (43°23′52″S, 65°2′55″W). All localities are in Chubut province, Patagonia, Argentina; Gaiman Formation (early Miocene; Mendía & Bayarsky, 1981; Scasso & Castro, 1999; see 'Geological setting' section for more details on the stratigraphic occurrence of the specimens).

Emended diagnosis: *Phoberodon arctirostris* differs from OU 21798, *Prosqualodon davidis* Flynn, 1923, *Squalodon calvertensis* Kellogg, 1923, *I. vertizi* and platanistoids (the contents of Platanistoidea of the present work are defined in the 'Phylogenetic analysis' section below) in the following unique combination of apomorphies: long and wide rostrum with wide premaxilla at mid-length, maxilla and premaxilla are unfused along the rostrum, medially straight mandible, absence of an antorbital process of maxilla, presence of an expanded tympanosquamosal recess (except *I. vertizi*), lacrimal restricted below the supraorbital process of maxilla (except *I. vertizi*), frontal forming the dorsolateral edge of the ventral infraorbital foramina (except *I. vertizi*), pointed postorbital process of frontal (except OU 21798), absence of a maxillary crest (except OU 21798) and convex ventral edge of zygomatic process (except *I. vertizi*). It further differs from *P. davidis*, *S. calvertensis* and platanistoids in having: a posterolateraly oriented postorbital process of frontal, wide right premaxilla posterior to premaxillary foramen, lack of a maxillary intrusion, shallow neck muscle fossa, most posterior portion of alisphenoid–squamosal suture anterior to foramen ovale and acromion horizontally oriented. *Phoberodon arctirostris* further differs from *P. davidis*, *S. calvertensis* and OU 21798 in having: a longitudinal groove on the ventral side of the mandible, an anteromedially oriented orbit and a dorsal infraorbital foramina near the posterior portion of the premaxilla. *Phoberodon arctirostris* differs from *P. davidis*, *S. calvertensis*, *I. vertizi* and platanistoids by having: a wide rostrum at the base (except *I. vertizi*), rostral constriction anterior to the maxillary flange, vertex

skewed to the left (except *I. vertizi*), a premaxillary foramen anterior to the antorbital notch (except *P. davidis* and *I. vertizi*) and squared-off postglenoid process of squamosal (except *P. davidis*). It differs from OU 21798, *S. calvertensis*, *I. vertizi* and platanistoids in having: the maxilla forming the posterior wall of the antorbital notch and in the moderately concave posterior sinus fossa. *Phoberodon arctirostris* differs from OU 21798 and platanistoids in the absence of a posterior portion of the periotic fossa. *Phoberodon arctirostris* further differs from *P. davidis* and *S. calvertensis* in having: a transversely inflated premaxilla at the rostrum, nasals with a concave posterior margin and presence of a supraspinous fossa of the scapula; and from OU 21798 and *S. calvertensis* in having a deep posterolateral sulcus. *Phoberodon arctirostris* differs from OU 21798 and *I. vertizi* in having a longer maxilla on the rostrum. It further differs from OU 21798 in having: three anterior dorsal infraorbital foramina, a dorsally exposed ethmoid, a shallow premaxillary cleft, an unfused mandibular symphysis and presence of a pterygoid sinus fossa anterior to the internal nares. *Phoberodon arctirostris* differs from *P. davidis* in having: striated tooth enamel, mandibular teeth of about the same size, a premaxilla of constant width along the cranium, lateral lamina of the palatine fused to the maxilla, shallow anterior slope of the scapula, a coracoid process not expanded distally plus a distally expanded acromion; and from *S. calvertensis* in having: teeth with an entocingulum, nasals at the same height as frontals, frontals forming the anterodorsal wall of the braincase, temporal fossa shorter than anteroposteriorly long, ventrally exposed palatine, and a dorsolaterally developed dorsal transverse process of the atlas. *Phoberodon arctirostris* differs from *I. vertizi* in having: the premaxillae widely separated by the mesorostral groove, presence of anteriorly oriented and procumbent incisors, both premaxillae extending posterior to nasals, presence of a premaxillary sac fossa, temporal fossa not roofed over by lateral expansion of the maxilla, and a wide external auditory meatus. It further differs from platanistoids and *I. vertizi* in having a high coronoid process on the mandible; and from platanistoids in having heterdont teeth with a short crown.

Physical maturity: The preserved cranial sutures are closed but distinct in all the specimens; in MPEF-PV 10883, the frontal–nasal suture is also closed. The external surface of the left occipital condyle preserved on the holotype and the articulation surfaces of the skull and scapula of all specimens, and the humerus and radius of the holotype have smooth surfaces, without the coarse pitting that might indicate juvenile bone. The nuchal crest is distinct in the holotype and MLP 5-3, but in MPEF-PV 10883 it is poorly developed (whether ontogenetic or postmortem bioeroded is uncertain). The epiphyses of all the vertebrae of the holotype and MPEF-PV 10883 are fused, and of all the vertebrae except three thoracic vertebrae (one of them has the epiphyses partly fused) and two lumbar vertebrae (one only the posterior epiphyses) of MLP 5-3 are fused. All these features suggest that *P. arctirostris* is represented by stage V individuals, following Perrin's (1975) stages for *Stenella attenuata* (Gray, 1846).

Body size: Given that none of the specimens has an articulated squamosal, we estimated the bizygomatic width of the holotype skull with the specimen on its metal mount. We applied the formula proposed by Pyenson & Sponberg (2011) for stem Odontoceti: $\log(TL) = 0.92 \times [\log(BIZYG) - 1.72] + 2.68$. The estimated bizygomatic width (BIZYG) of *P. arctirostris* is 331 mm, giving a reconstructed total length (TL) of 3.13 m, that is, a little more than three times the cranial length. Cabrera reported a holotype skull length of 994 mm, whereas we obtained 1200 mm. Also, Cabrera (1926: 389) indicated a body length of ~4.25 m. If we sum the skull condylobasal length (CBL) plus the length of all the vertebrae preserved, we estimate a total length of 3.3 m for the holotype and 3.1 m for MLP 5-3. Given that the postcranial skeleton is incomplete, the estimated total length from the formula of Pyenson & Sponberg (2011) might be slightly underestimated. Nonetheless, the estimated total length is comparable amongst living odontocetes to *Delphinapterus leucas* Pallas, 1776, *Pseudorca crassidens* Owen, 1846, *Mesoplodon hectori* Gray, 1871 and *Kogia breviceps* de Blainville, 1838, among others (Perrin *et al.*, 2008).

Description

Skull general description

The holotype MLP 5-4 skull has a CBL of 1200 mm, MLP 5-3 has a CBL of 830+ mm and MPEF-PV 10883 of 1230+ mm. Thus, *P. arctirostris* has, together with *Zarhachis flagellator* Cope, 1868 (CBL = 1195 mm; Kellogg, 1924), one of the longest skulls among stem odontocetes and platanistoids (for the contents of Platanistoidea see 'Phylogenetic analysis' section), longer than *Platanista gangetica* Lebeck, 1801 (average CBL = 449 mm; Anderson, 1878), *Squalodelphis fabianii* Dal Piaz, 1917 (CBL = 645+ mm; Dal Piaz, 1917), *W. maerewhenua* (CBL = 556+ mm; Fordyce, 1994) and even *Pomatodelphis inaequalis* Allen, 1921 (CBL = 925+ mm; Kellogg, 1959). It is also longer than the skull of *S. calvertensis* (CBL = 750 mm; Kellogg, 1923), *P. davidis* (CBL = 548 mm; Flynn, 1948), *I. vertizi* (CBL = 940 mm; Lambert *et al.*, 2018) and *Macrosqualodelphis ukupachai* Bianucci et al., 2018 (CBL = 770+ mm; Bianucci *et al.*, 2018).

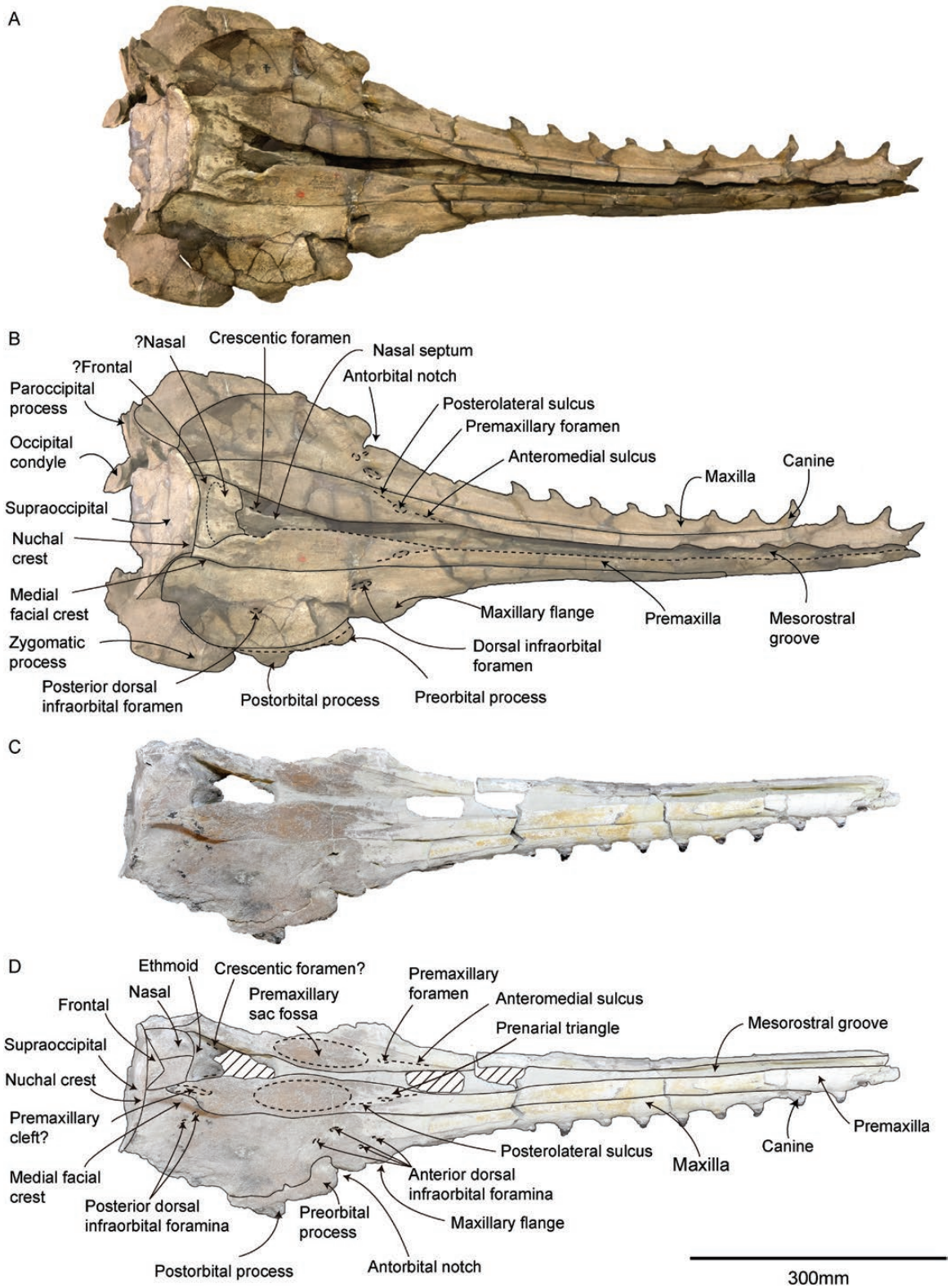

Figure 2. Dorsal view of skull of *Phoberodon arctirostris*. A, B, MLP 5-4 (holotype). C, D, MPEF-PV 10883. Dashed lines indicate specific structures, and continuous lines indicate sutures. Hatched outlines show broken areas of the specimen. Note that fine dashed lines indicate uncertain sutures.

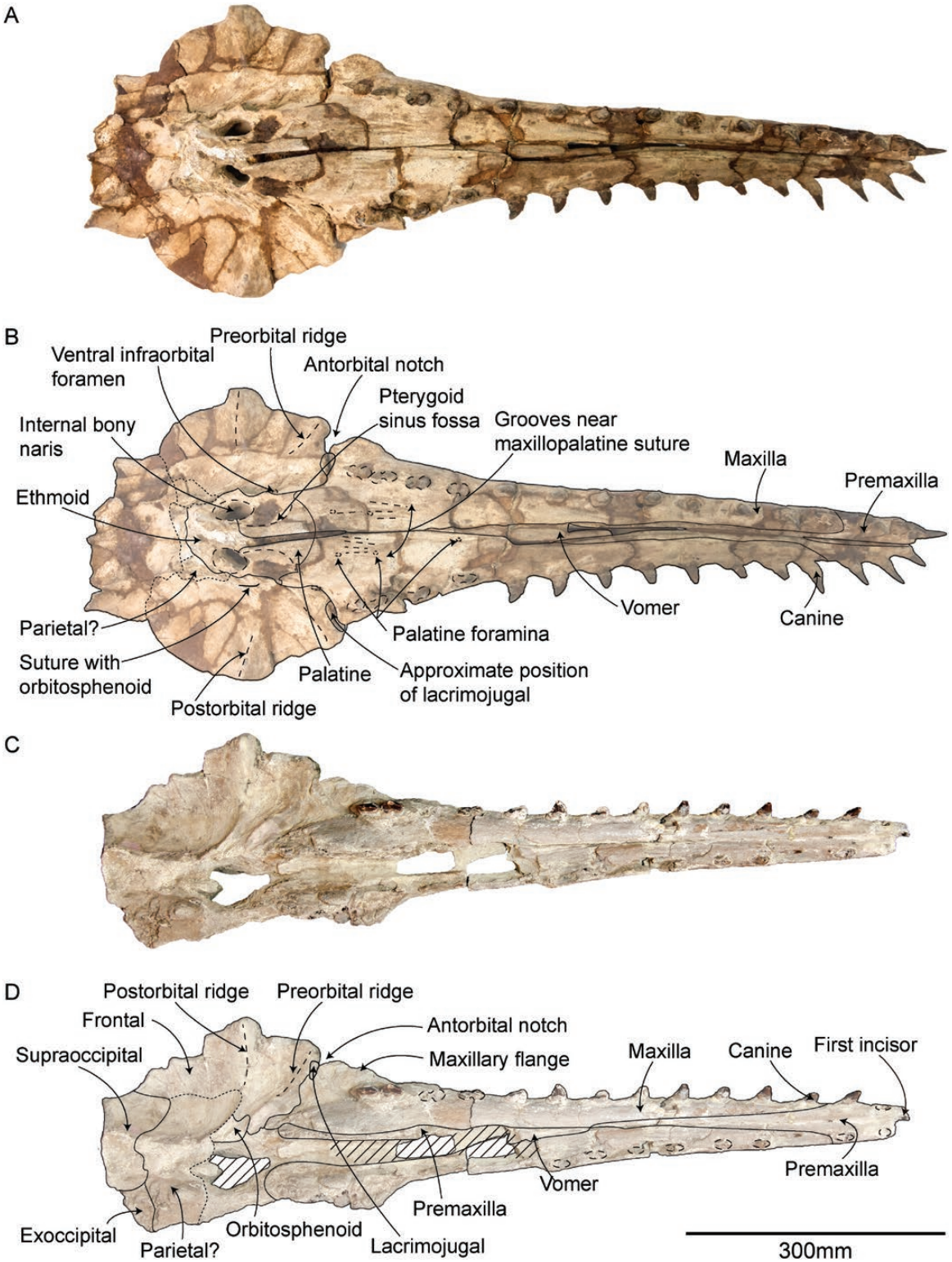

Figure 3. Ventral view of skull of *Phoberodon arctirostris*. A, B, MLP 5-4 (holotype). C, D, MPEF-PV 10883. Dashed lines indicate specific structures, and continuous lines indicate sutures. Hatched outlines show broken areas of the specimen. Note that fine dashed lines indicate uncertain sutures.

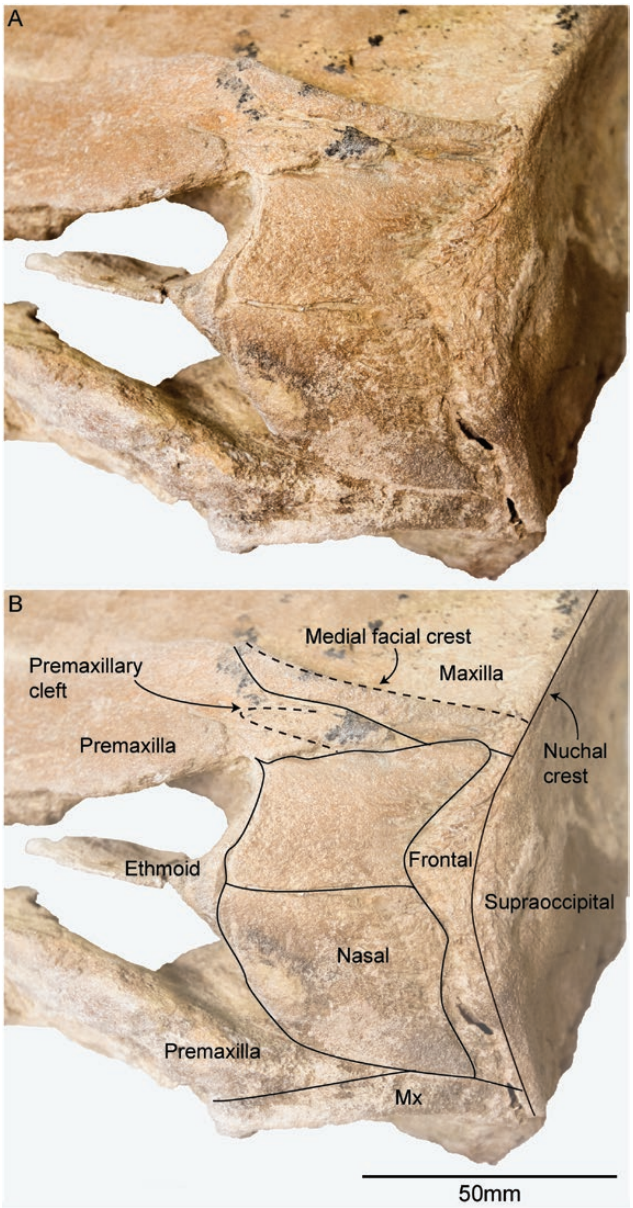

Figure 4. Dorsal view of vertex area of *Phoberodon arctirostris*. A, B, MPEF-PV 10883. Dashed lines indicate specific structures, and continuous lines indicate sutures.

Rostrum: The rostrum is long, wide at its base at the antorbital notches, and anteriorly narrow and attenuated, contributing ~60% of CBL (Table 1). In lateral view, it is slightly convex dorsally, with the matching profile of the mandible indicating that the curve is original, not postmortem. The antorbital notch is V shaped, and longer anteroposteriorly than wide (Table 1). It is oriented anterolaterally, thus having the anteroposterior axis of the antorbital notch forming an acute angle with the sagittal axis of the skull (in *P. gangetica*, both axes are parallel). The open mesorostral groove is narrow anteriorly and it widens posteriorly, and about the external nares it narrows again. It is bounded laterally by the premaxilla and ventrally by the vomer. The maxilla and premaxilla are in contact throughout their length, and the suture is grooved. In ventral view, the exposure of the premaxilla decreases in a posterior direction, and only a small portion of the vomer is visible at the posterior portion. In all specimens, the rostrum was more compressed on one side and presents a leftward deviation.

Cranium: It is short anteroposteriorly and wide laterally (Table 1). The external nares are longer

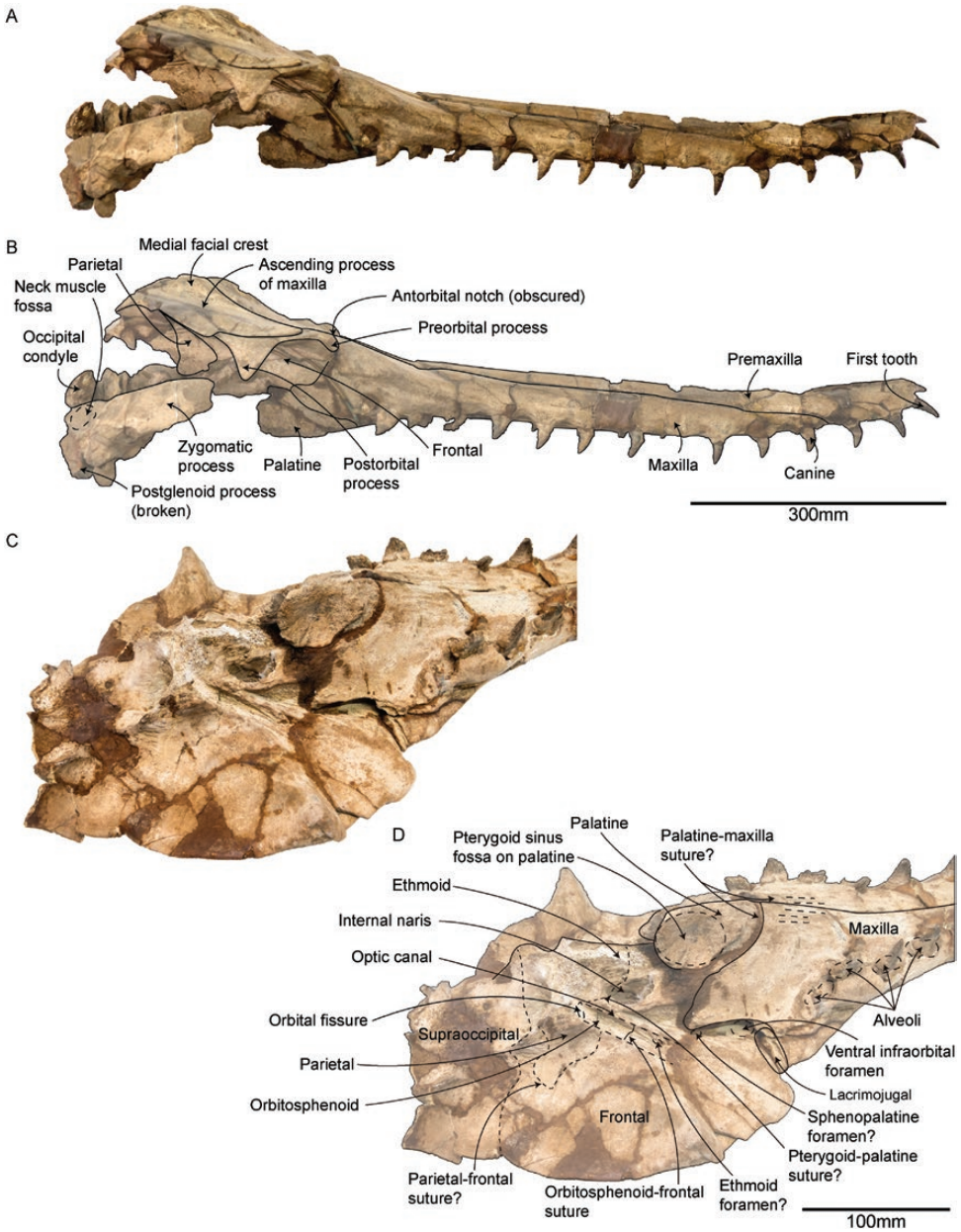

Figure 5. Lateral (A, B) and posterolateral (C, D) views of skull of *Phoberodon arctirostris*, MLP 5-4 (holotype). Dashed lines indicate specific structures, and continuous lines indicate sutures. Note that fine dashed lines indicate uncertain sutures.

anteroposteriorly than narrow transversely, with a rectangular profile (Table 1). In dorsal view, the maxilla and premaxilla are extensively developed laterally to the external nares and form a high medial facial crest (*sensu* Fordyce, 1994) lateral to the nasals and frontals. In lateral view, the vertex is little elevated posterodorsally with respect to the dorsal surface of the rostrum; thus, the cranium seems low. The vertex is formed by the nasals, frontal, premaxilla and maxilla; it is slightly asymmetrical, and shifted to the left side (asymmetry: +20.31 mm; skew: +1.69; see Ness (1967) for methodology). The premaxillary sac fossae are longer than wide and have no visible asymmetry.

Premaxilla (Figs 2–6): In dorsal view, the premaxilla laterally contacts the maxilla, and medially the nasal, frontal (except MPEF-PV 10883) and the ethmoid. It variably contacts posteriorly with the supraoccipital. The premaxilla is slightly expanded laterally at the tip of the rostrum, where it carries incisor (I)1–3 and

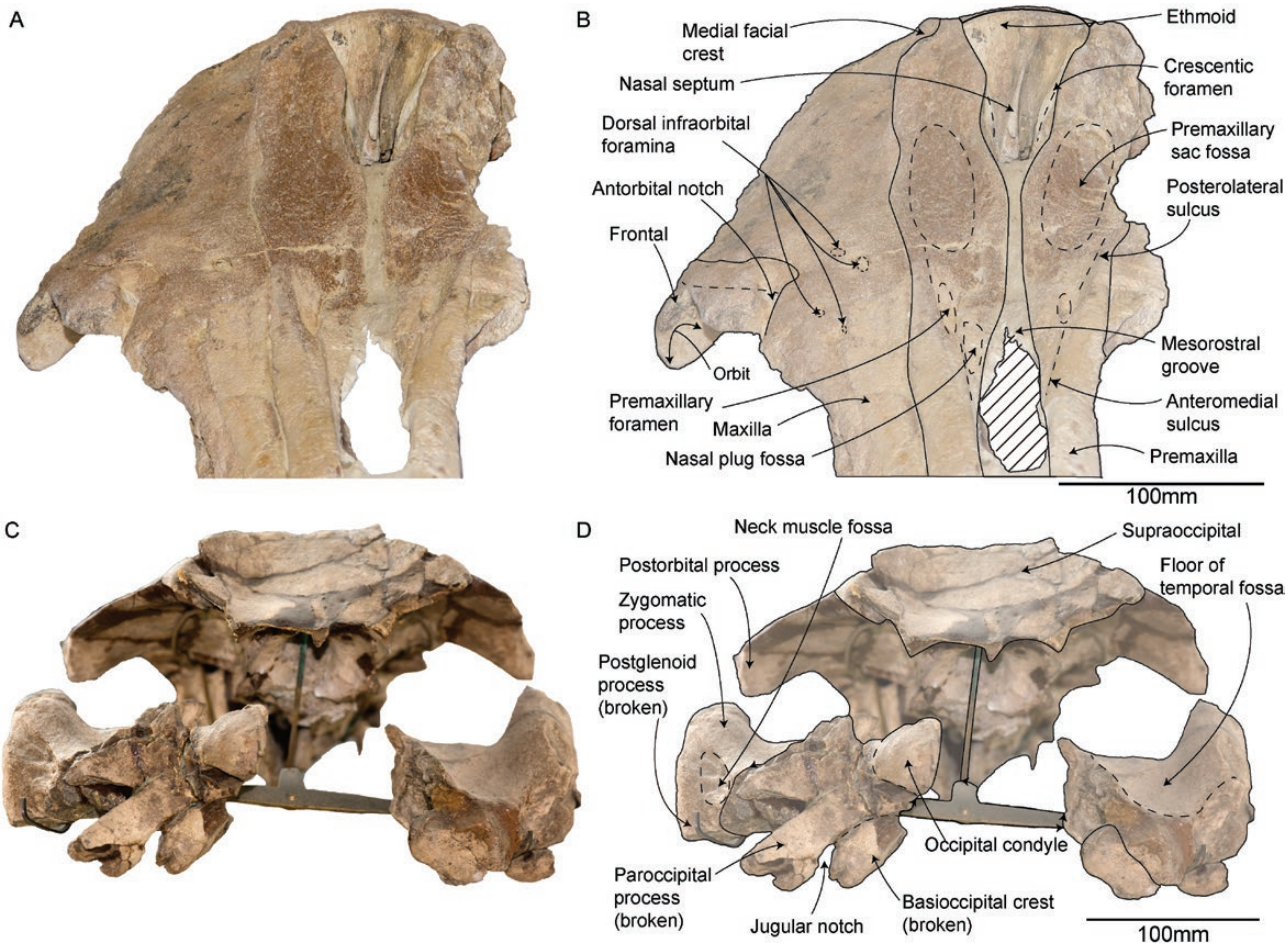

Figure 6. Anterior (A, B) and posterior (C, D) views of skull of *Phoberodon arctirostris*. A, B, MPEF-PV 10883. C, D, MLP 5-4 (holotype). Dashed lines indicate specific structures, and continuous lines indicate sutures.

excludes the maxilla (MLP 5-4: 139.5 mm), similar to *S. calvertensis* and *I. vertizi* but unlike *M. ukupachai*. Then, it narrows posteriorly to about mid-rostral length (Table 1), widening again posterior to the antorbital notch. The medial margin of the premaxilla partly roofs the full length of the mesorostral canal without bilateral contact, similar to *S. calvertensis* but unlike *M. ukupachai*, whilst the posterior portion bounds the external nares laterally. In ventral view, the premaxilla is exposed on the anterior half of the rostrum and narrows posteriorly, only contacting along the most anterior portion. In lateral view, the dorsal surface of the premaxilla is slightly convex along the rostrum.

The premaxillary foramen opens anterior to the antorbital notch, more anteriorly than in *M. ukupachai*. It is longer anteroposteriorly than wide, but without marked asymmetry (Table 1). The foramen opens into anteromedial and posterolateral sulci (the latter more markedly so in MLP 5-3 and in MPEF-PV 10883) that extend at least to the antorbital notch. The posteromedial sulcus could not be identified. The prenarial triangle (origin for the nasal plug muscle) is present immediately anterior to the premaxillary foramen. The premaxillary sac fossa is located posteromedially along the premaxilla, posterior to the premaxillary foramen, and it is longer than wide, with no visible asymmetry (Table 1). The medial and lateral margins of this fossa are convex (more markedly so in MPEF-PV 10883), and the smooth dorsal surface is flat in lateral view. Posteriorly, the nasal process of the premaxilla is longer than wide, with the medial and lateral margin also convex. MPEF-PV 10883 presents a slight prenarial constriction (*sensu* Fordyce, 1994). There is a marked narrowing of the premaxilla between the nasal process and the premaxillary sac fossa. In lateral view, the nasal process is little elevated towards the vertex of the skull. A shallow premaxillary crest is identified in the holotype and MPEF-PV 10883, similar to *W. maerewhenua* and *M. ukupachai*. Posterodorsally, a posteromedial splint of premaxilla medially contacts the nasal and the

frontal, and laterally contacts the maxilla through a visible but closed suture. In MPEF-PV 10883, the premaxilla extends posterodorsally to the nasofrontal suture (similar to *M. ukupachai*), but in the holotype and MLP 5-3 it contacts the supraoccipital. At the level of the nasal process, together with the maxilla, they form a blunt and robust medial facial crest (*sensu* Fordyce, 1994), lateral to the nasals and frontals on the vertex. This crest is more prominent on the right side in the holotype and MPEF-PV 10883 (but on the left side for MLP 5-3).

Maxilla (Figs 2–6): In dorsal view at the rostrum, the maxilla contacts the premaxilla medially through a deeply grooved unfused suture, similar to *W. maerewhenua* but contrary to *M. ukupachai*. Contacts on the cranium include: posteriorly with the supraoccipital (suture visible only in MPEF-PV 10883), posteromedially with the premaxilla (and frontal in MPEF-PV 10883), and ventrally at the orbit with the frontal and lacrimojugal. The maxilla is narrow anteriorly in dorsal view (width at half length of rostrum, MLP 5-4: 38.3 mm) and it widens posteriorly (width at antorbital notch, MLP 5-4: 84 mm). The dorsal surface of the maxilla is slightly concave on the rostrum, becoming flat posteriorly. The antorbital notch is formed by the maxilla and the frontal in dorsal view (as in *S. calvertensis*), and by the maxilla and lacrimojugal in ventral view; the notch is anterolaterally oriented and has a 'U' shape. In dorsal view, along the dorsal surface of the maxilla and anterior to or at the antorbital notch are the dorsal infraorbital foramina, which vary from one to three on the left side and from one to four on the right, more than in *M. ukupachai*. Additionally, MPEF-PV 10883 has two posterior dorsal infraorbital foramina, lateral to the medial facial crest, whereas MLP 5-3 has only one. Anterior to the antorbital notch and lateroposterior to the last alveoli is the maxillary flange, with a concave lateral margin. In ventral view, the maxilla bears 13–15 alveoli on the right side and eight to 15 alveoli on the left side (Table 1). The last four or five alveoli seem to be for double-rooted teeth, and the remaining alveoli are for single-rooted teeth.

In dorsal view at the cranium, the ascending process of the maxilla contacts posteromedially with the nasal process of the premaxilla through a visible but closed suture. Given that the ascending process of the maxilla was broken on one side in all specimens, no asymmetry was observed. In lateral view, the ascending process of the maxilla does not present an accentuated posterodorsal elevation, and the dorsal surface is slightly concave. At the orbit, the maxilla does not completely cover the frontal, leaving it exposed, similar to *S. calvertensis* and *M. ukupachai*. The ventral infraorbital foramen is preserved only on the holotype, posteromedial to the antorbital notch. The ventral margin is formed by the maxilla, and the dorsal margin by the frontal and, possibly, lacrimojugal.

Palatine (Figs 3, 5; Supporting Information, Appendix S5): In ventral view, the palatine contacts anterolaterally with the maxilla. Some marked grooves at about the antorbital notch and the presence of foramina anteriorly indicate the approximate position and extension of this suture. Ventrolaterally, each palatine contacts the pterygoid. The palatines appear separated by the vomer. The palatine extends anteriorly at about or just posterior to the last alveolus, similar to *I. vertizi* and *S. calvertensis*, and posteriorly up to the ventral portion of the anterior wall of the internal nares. The palatine may form the medial wall of the pterygoid sinus fossa; however, the pterygoid is not preserved well enough to be certain. Posteriorly to the ventral infraorbital foramina and anteromedial to the optic canal, there is a foramen tentatively assigned as the sphenopalatine foramen.

Nasal (Figs 2, 4): In dorsal view, the nasal is mainly trapezoidal, wider than long (Table 1), with a slight asymmetry that varies on each specimen. The internarial suture is straight and visible. The slightly concave anterior margin of the nasal contacts the ethmoid through a visible but closed suture. Posteriorly, it contacts the frontal through a completely fused V-shape suture, with a rugose area immediately anterior to the suture. Laterally, it contacts the premaxilla through a visible suture. The nasals form the major portion of the vertex, whereas they are smaller in *S. calvertensis*, *W. maerewhenua*, *I. vertizi* and *M. ukupachai*. In lateral view, the dorsal surface of the nasal is flat and at the same level as the frontal. The nasal does not overhang but is slightly elevated about the external bony nares.

Ethmoid (Figs 3, 4, 6; Supporting Information, Appendix S5): The ethmoid forms the posterior wall of the nasal passage, contacting the nasal and premaxilla dorsally and the vomer anteroventrally. In anterior view, it has a robust anteroposteriorly and dorsoventrally developed nasal septum or mesethmoid [but note that Ichishima (2016) suggested there might be no mesethmoid in cetaceans], markedly shifted to the left; it is similar to *W. maerewhenua* and *M. ukupachai*. Lateral to the mesethmoid are the cribriform plates, with concave surfaces, forming the posterior wall of the nasal passages. The cribriform plate of the holotype and MPEF-PV 10883 presents a crescentic foramen immediately lateral to the nasal septum, which could represent the vestige of the passage of a primary olfactory axon (Godfrey, 2013).

Lacrimojugal (Figs 3, 5; Supporting Information, Appendix S5): This is currently not preserved in the holotype. However, Cabrera (1926) figured it on p. 381 and on p. 380 commented: 'cuando se mira el cráneo de perfil no oculta la base del yugal, como ocurre en *S. bariensis*. El lagrimal está metido, por decirlo así, en el ángulo que dicha apófisis [preorbital] forma con el maxilar' [when you look at the skull in lateral view, the base of the jugal is not hidden as in *S. bariensis*. The lacrimal is inserted, so to speak, on the angle that said apophyses (preorbital) forms with the maxilla]. At present, only the fossa where the lacrimojugal would be lodged can be identified. It appears that it contacted the maxilla dorsally, medial to the antorbital notch, and also contacted the tip of the zygomatic process of the squamosal, on its ventral side, similar to *I. vertizi*. MPEF-PV 10883 has a portion of the right lacrimojugal preserved at the same position, forming the ventral margin of the antorbital notch with the maxilla, as in *M. ukupachai*.

Vomer (Fig. 3): It forms the floor of the mesorostral canal and contributes to the ventral margin of the nasal septum. The vomer contacts the premaxilla dorsally, the maxilla laterally and the palatine (and perhaps pterygoid) ventrally. There is a very narrow exposure of the vomer ventrally, from about half the rostrum length up to the posterior cheek teeth, separating the premaxillae. Posteriorly, the vomer is covered by the palatine and maxilla, and it is again visible medial and posterior to the internal nares, similar to *I. vertizi*.

Frontal (Figs 2–6; Supporting Information, Appendix S5): The frontal contacts the nasal anteriorly at a closed suture, the premaxilla (or maxilla in MPEF-PV 10883) laterally through a visible but closed suture, the supraoccipital posteriorly with a fused suture, and the maxilla dorsally above the orbit region. At the vertex in dorsal view, the frontal is wider than longer anteroposteriorly (Table 1), with a narial process invading the right nasal. In lateral view, the surface of the frontal is flat. At the orbital region, the frontal delimits the antorbital notch lateroventrally and the dorsal margin of the orbit. In lateral view, the preorbital process of the frontal is robust, dorsoventrally thickened and anteroposteriorly oriented, parallel to the sagittal plane of the skull; it is similar to *S. calvertensis* and *I. vertizi*. The triangular, blunt and mediolaterally thickened postorbital process of the frontal is larger than the preorbital process, and ventrally oriented; it is longer and more robust in *M. ukupachai* and sharper in *S. calvertensis*. In constrast, the preorbital process is anteriorly oriented. In dorsal view, the anteroposterior axis of the orbit (from the preorbital to the postorbital process) forms an acute angle with the sagittal axis. In ventral view, the frontal contributes to the dorsal margin of the infraorbital foramina. At the orbit, the surface of the frontal bears the preorbital and postorbital ridges, with the latter being the most pronounced. Between both ridges, the triangular roof of the orbit is anteroposteriorly long and deep, and the resulting orbit is wider than in *M. ukupachai* but similar to *S. calvertensis* and *I. vertizi*. The optic canal is narrow ventrally and wider dorsally, and it has an anterolateral orientation. The ventral portion of this canal is formed by the orbitosphenoid. No fossae for the preorbital or postorbital lobe of the pterygoid sinus were identified, contrary to *M. ukupachai*.

Parietal (Figs 3, 5, 7; Supporting Information, Appendix S5): In dorsal view, the partly preserved parietal forms the posterior wall of the temporal fossa, with a closed parietosquamosal suture posteriorly. At the basicranial region, in ventral view, the parietal is medial to the falciform process of the squamosal and anterior to the exoccipital, as well as anteromedial to the alisphenoid. There is no contribution of the parietal to the periotic fossa. The posterior lacerate foramen is medial to the foramen spinosum and lateral to the basioccipital crest. In ventral view at the roof of the cranium there is also a contribution of this bone.

Supraoccipital (Figs 2, 4, 6; Supporting Information, Appendix S5): The partly preserved supraoccipital projects anteromedially towards the vertex, where it contacts the frontal, premaxilla and maxilla with a completely fused suture. In posterior view, the dorsal surface is slightly concave and ventrally inclined. The lateral margins are posteriorly oriented and convex, similar to *W. maerewhenua*. The convex nuchal crest is poorly developed in MPEF-PV 10883, being at the same plane as the vertex, contrary to *M. ukupachai*. The nuchal crest is more convex in *S. calvertensis*.

Exoccipital (Fig. 6; Supporting Information, Appendix S5): In posterior view, the occipital condyles have a round shape, and it appears they were prominent, smaller than in *I. vertizi* and similar to *M. ukupachai*. The paroccipital process is lateral to the jugular notch, dorsoventrally short with a rounded apex, and less developed than in *I. vertizi*. In ventral view, the anteromedial surface of this process has a distinct fossa, immediately posterior to the periotic fossa. In odontocetes, there are at least two bony correlates of the pterygoid sinus system in the exoccipital: one corresponds to the posterior sinus (in the anteroventral surface of the paroccipital process) and the other to the posterolateral extension of the peribullary sinus (ventral surface of paroccipital process; Mead & Fordyce, 2009). The identification of these bony correlates is confusing in the literature, because the posterior sinus fossa is variably developed (Fraser &

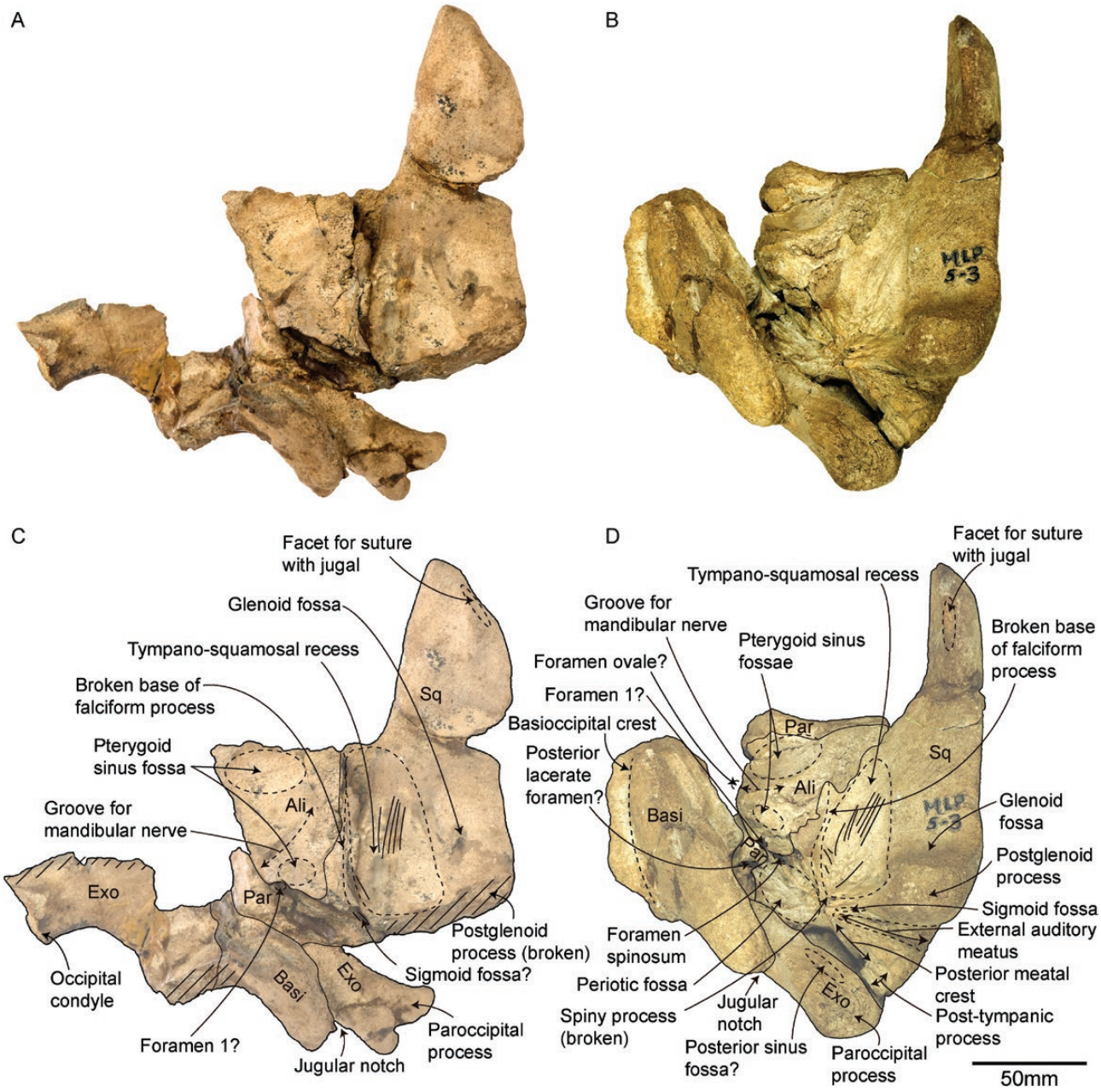

Figure 7. Ventral view of squamosal of *Phoberodon arctirostris*. A, C, MLP 5-4 (holotype). B, D, MLP 5-3. Dashed lines indicate specific structures, and continuous lines indicate sutures. Hatched outlines show broken areas of the specimen. Abbreviations: Ali, alisphenoid; Basi, basioccipital; Exo, exoccipital; Par, parietal; Sq, squamosal.

Purves, 1960; Fordyce, 1994). Based on the anatomical location of the fossa in *P. arctirostris*, it is tentatively identified as the posterior sinus fossa, whereas it is absent in *I. vertizi* and *W. maerewhenua*. There is no obvious evidence of articulation of the paroccipital processes with the stylohyoid. The jugular notch is well defined and fairly deep, but it is shallower than in *S. calvertensis* and *I. vertizi*.

Squamosal (Figs 2, 5, 6, 7): In all specimens, this is only partly preserved and disarticulated from the skull. In dorsal view, the anteriorly oriented zygomatic process is longer than wide (as noted by Cozzuol, 1996; Table 1), with a straight dorsal margin and convex ventral margin. In lateral view it is strongly swollen, similar to *S. calvertensis*, longer than *Otekaikea* spp. and *I. vertizi* but shorter than *M. ukupachai*, and with

a blunt anterior tip. In posterolateral view, a triangle-shaped neck muscle fossa (*sensu* Fordyce, 1981) is located posterior to the zygomatic process, dorsal to the postglenoid process and anterior to the exoccipital; distinct crests delimit this fossa, which is oriented anteroposteriorly. This fossa can also be seen, for example, in *S. calvertensis*, *W. maerewhenua*, *Otekaikea* spp., *Aondelphis talen* Viglino et al., 2018 and *I. vertizi*. The prominent postglenoid process is ventrally oriented and triangular in shape, with a blunt apex (also noted by Cozzuol, 1996). The postglenoid process is more prominent than in *S. calvertensis*, *A. talen*, *Otekaikea* spp. and *W. maerewhenua*.

In ventral view, the squamosal contacts the exoccipital posteriorly and the alisphenoid and parietal medially. A presumed suture for the jugal is located on the anterolateral margin of the zygomatic process, similar to *S. calvertensis* and *M. ukupachai*. The mandibular fossa is anteroposteriorly long, shallow and narrow. The deep and wide tympanosquamosal recess, which lodges the middle sinus of the pterygoid sinus system (Fraser & Purves, 1960), extends anteroposteriorly along the ventral surface of the zygomatic process of the squamosal and ventrolaterally to the medial surface of the postglenoid process, as noted by Cozzuol (1996). It is wider than in *M. ukupachai* and of similar extent to *A. talen*. The recess also presents several parallel ridges, anterolaterally and posteromedially oriented. The base of the falciform process has a sigmoid profile, similar to *S. calvertensis*. Posterolaterally, there is a shallow but distinct oval-shaped sigmoid fossa (*sensu* Geisler *et al.*, 2005). The well-developed anterior meatal crest delimits the tympanosquamosal recess posteriorly; and the posterior meatal crest is less developed and anterior to the post-tympanic process. Together, they define the narrow external acoustic meatus, which is wider laterally and narrows medially. The meatus is deeper than in *Otekaikea* spp., similar to *N. vanbenedeni*, narrower than in *S. calvertensis* but wider than ZMT-73, *A. talen* and *I. vertizi*. Posteriorly is the short post-tympanic process, with striations that would indicate a point of contact with the tympanic bulla, similar to *I. vertizi*. However, given that the tympanic bulla and periotic are still unknown for this species, no certain assessments can be made. The broken spiny process was recognized on the holotype, medial to the external acoustic meatus and posterior to the tympanosquamosal recess. The shallow and rounded periotic fossa is shallower than in *Otekaikea* spp. and *W. maerewhenua*. There is no contribution of the parietal to the fossa and no visible supratubercular ridge. There are some striations on the anteromedial area of the periotic fossa, which could correspond to a point of contact with the anterior process of the periotic. The foramen spinosum is within the periotic fossa, medial to the falciform process, immediately posterior to the alisphenoid–squamosal suture and lateral to the parietal; the alisphenoid contributes to the anterior margin of this foramen. This interpretation of the foramina differs from that of Cozzuol (1996). We could not identify a subcircular fossa (*sensu* Viglino *et al.*, 2018) for *P. arctirostris*, contrary to what Cozzuol (1996) indicated.

Orbitosphenoid and alisphenoid (Figs 3, 5, 7; Supporting Information, Appendix S5): In ventral view at the orbit region, the orbitosphenoid forms the ventroposterior portion of the optic canal, apparently contacting the vomer medially and the frontal laterally. Immediately anterior to the orbitosphenoid–frontal suture, on the left side of the holotype, the ethmoid foramen can be recognized. On the most posterior portion of the optic canal and lateral to the internal nares might be a partly preserved orbital fissure.

In ventral view of the basicranium, the alisphenoid contacts the parietal anteriorly and posteriorly, and the squamosal laterally. It forms the anterior margin of the foramen spinosum. Two distinct fossae for the pterygoid sinus system can be recognized, whereas a single fossa was observed in *W. maerewhenua*; the anterior one is located posterior to the parietal and medial to the tympanosquamosal recess of the squamosal (as described by Cozzuol, 1996). The posterior fossa is located anterior to the parietal and foramen spinosum, and medial to the falciform process of the squamosal. The alisphenoid probably forms the lateral margin of the foramen ovale (not preserved), followed by a groove for the mandibular nerve; it is similar to *W. maerewhenua*. Anterior to the foramen spinosum, at the alisphenoid–parietal suture, there is a foramen tentatively homologized with foramen 1 of *W. maerewhenua* (*sensu* Fordyce, 1994).

Teeth (Fig. 8): *Phoberodon arctirostris* is heterodont and polydont. There are 15 upper teeth on each side (three teeth in the premaxilla and 12 in the maxilla), and 13+ in each mandible (Tables 1 and 2), similar to *P. davidis* and slightly fewer than in *W. maerewhenua* and *I. vertizi*. The teeth are single rooted, except the last five upper cheek teeth and the last four lower cheek teeth, which are double rooted; this is unlike the condition of all single-rooted teeth of *Otekaikea huata* Tanaka & Fordyce, 2015 and *M. ukupachai*. For MPEF-PV 10883, the seventh cheek tooth is the first upper double-rooted tooth; also, the last cheek tooth has a possible fused third root in lingual view. The first three upper teeth (i.e. incisors) present a conical crown with low and separated subparallel enamel ridges, and they are all inserted in the premaxilla, similar to *Waipatia hectori* Tanaka & Fordyce, 2015, *I. vertizi* and *Otekaikea marplesi* Tanaka & Fordyce, 2014; the apex variably presents abrasional wear facets (Loch & Simões-Lopes, 2013). I1

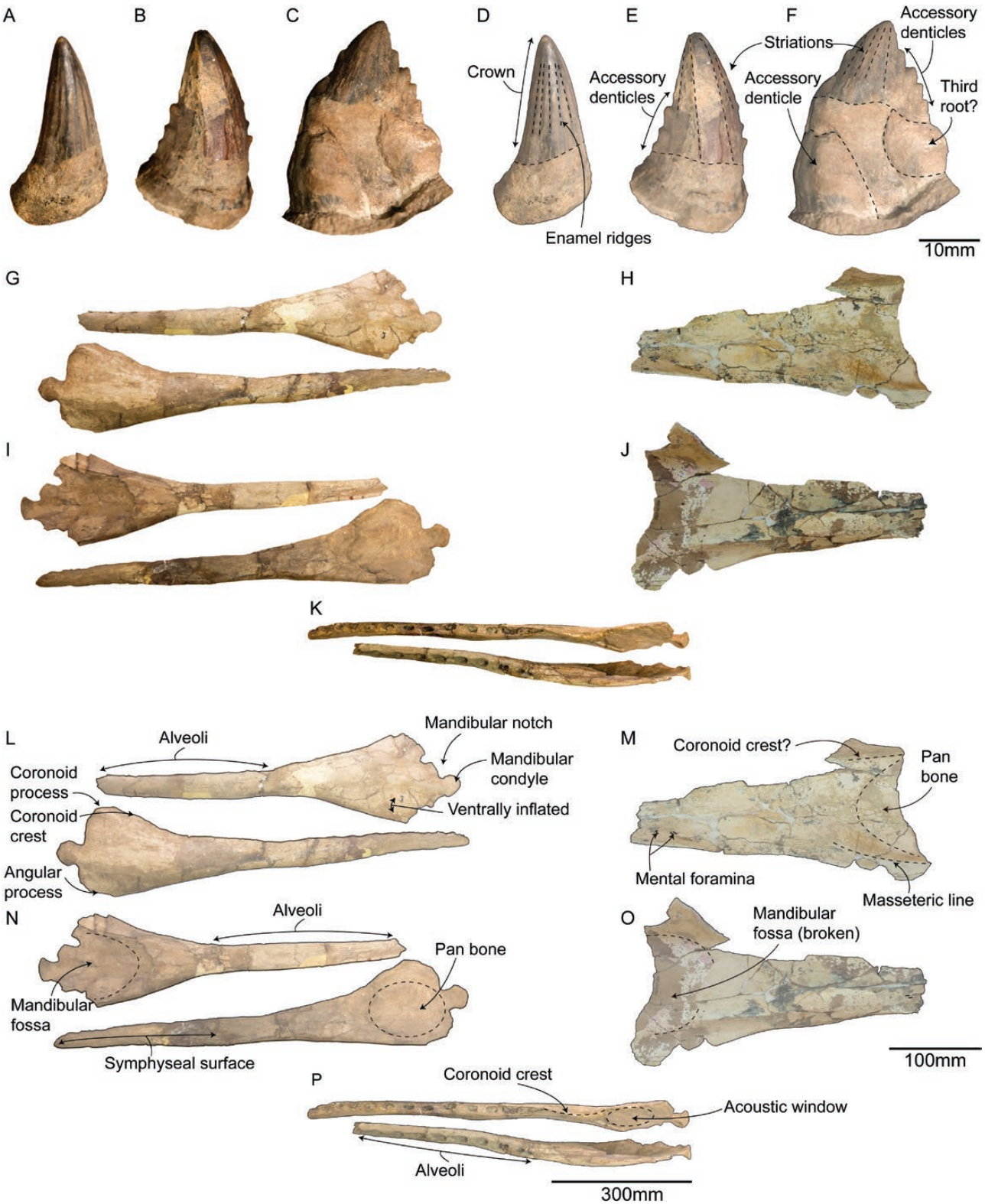

Figure 8. Mandible and teeth of *Phoberodon arctirostris*. (A-F) MLP 5-4 (holotype); (G,I,K,L,N,P) MLP 5-3; and (H,J,M,O) MPEF-PV 10883. For teeth, photographs correspond to (A,D) incisor, (B,E) middle cheek-teeth and (C,F) posterior cheek-teeth, all in labial views. For the mandibles, (G,H,L,M) lateral, (I,J,N,O) medial and (K,P) dorsal views. Dashed lines indicate specific structures.

is procumbent and anteriorly oriented, whilst I2 and I3 have a more lateral orientation, similar to *P. davidis*, *W. hectori* and *I. vertizi*. I3 is curved buccally, with the apex pointing medially. In the maxilla, the subsequent canine and upper cheek teeth present a conical crown, with subparallel and widely separated enamel striations, an anterior and posterior keel, and the apex is ventrally oriented. These teeth are subcircular in cross-section and buccally curved, similar to *O. marplesi* and *P. davidis*. The most posterior upper cheek teeth present a more buccolingually compressed crown, resulting in a triangular profile, and are oriented posteroventrally, with variably developed accessory denticles (but always more and higher on the posterior margin, as in *Waipatia* spp.), more prominent on MPEF-PV 10883. This is also similar to the morphology of cheek teeth observed in *I. vertizi*, but this species has more developed accessory denticles. The enamel presents higher but more separated striations, especially on the lingual side, similar to *P. davidis*. The three most posterior upper cheek teeth are slightly shorter, ventrally oriented and more medially placed on the maxilla. Accessory denticles appear on the posterior teeth, first on the posterior margin; there are one to four on the anterior margin and three to five on the posterior margin, more than in *P. davidis*. Some denticles may present a wear facet (Loch & Simões-Lopes, 2013). Diastemata are markedly reduced posteriorly (Table 2). The same morphological variation described is present on the lower teeth.

The holotype specimen presents two anterior bilaterally symmetrical accessory denticles (lingually and buccally) on the last upper cheek tooth and the last two lower teeth (Cabrera 1926: fig. 12). These denticles do not resemble the shape or size of the accessory denticles described above. MPEF-PV 10883 does not present this characteristic.

Mandible (Fig. 8): The mandible is gracile and dorsoventrally low almost throughout its length, with a marked height increase towards the coronoid region. The mandibles are compressed laterally but are thicker than in *O. marplesi* and longer than in *P. davidis*. In dorsal view, the mandible has a convex lateral surface and a straight medial surface. The body of the mandible presents dental alveoli (Table 1), contrary to *Awamokoa tokarahi* Tanaka & Fordyce, 2017, and a long mandibular symphysis (almost half the mandibular length; Table 1; similar to *I. vertizi*); whether closed or not is uncertain because of obscuring glue. The alveoli are subcircular anteriorly, and posteriorly become elongated anteroposteriorly; they are all located along a straight axis, contrary to *P. davidis*. In lateral view, there are two or three foramina on the labial side of the mandible that correspond to the mental foramina, fewer than in *O. huata* and *I. vertizi*. Posterior to the last alveoli, the mandible is ventrally inflated, and the pan bone extends ventrally beyond the level of the body of the mandible. The coronoid process is small but robust and oriented posteriorly; a coronoid crest runs from this process towards the anterior end of the body of the mandible, similar to *O. huata* (and more developed than in *A. tokarahi*). The mandibular condyle is preserved only on MLP 5-3; it projects posteriorly, distinctly separated from the ramus by a well-defined neck, and it has a rounded outline (Table 1), similar to *P. davidis*. In posterior view, the condylar articular surface is round and smooth, and the mandibular notch is very pronounced. In medial view, the angular process of the mandible is small and oriented posteroventrally, and MPEF-PV 10883 presents a marked masseteric line anteriorly. The mandibular foramen is longer anteroposteriorly than dorsoventrally (Table 1). At this level, the transverse width of bone is the thinnest.

Postcranial skeleton

Atlas (Fig. 9): The atlas is not fused with the axis. It is robust, wide and long anteroposteriorly (Table 3). In dorsal view, the neural spine is short and low, less developed than in *O. marplesi*. In posterior view, there is a bilateral pair of large and transversally long upper transverse processes and a pair of short lower transverse processes (shorter than in *I. vertizi*). These processes are not connected to each other. The articular surfaces for the occipital condyles are distinctly separated dorsally and nearer ventrally. The neural canal is higher than wide, similar to *O. marplesi*. Ventrally, there is an anteroposteriorly long and posteriorly oriented hypapophysis, similar to *O. marplesi* but less developed than in *M. ukupachai*. In lateral view, there are vertebrarterial foramina anterior and posterior to the upper transverse process, the former being the smallest. In dorsal view, the large foramen for the first spinal nerve lies in the centre of the neural arch, as in *M. ukupachai*. The bilateral articular facets for the axis are flat and present a deep fossa (Fossa? in Fig. 9B) on the medial margin, possibly a point of contact with the axis. Medial to the facet for the axis is the tubercle for insertion of the transverse ligament. The fossa for the odontoid process is shallow.

Axis (Fig. 9): The axis is incomplete and is not fused to any adjacent vertebrae, like *Otekaikea* spp., *I. vertizi* and *M. ukupachai*. In anterior view, the long and posteriorly oriented right transverse process is preserved, as well as parts of the articular facets for the atlas, which are concave and short. The transverse process is narrower and longer than in *O. huata*. In ventral view, the anterior portion of the body of the axis is depressed and smooth, whereas the posterior portion has a weak medial crest. Cabrera (1926) made a possible reconstruction of this vertebra on his original description.

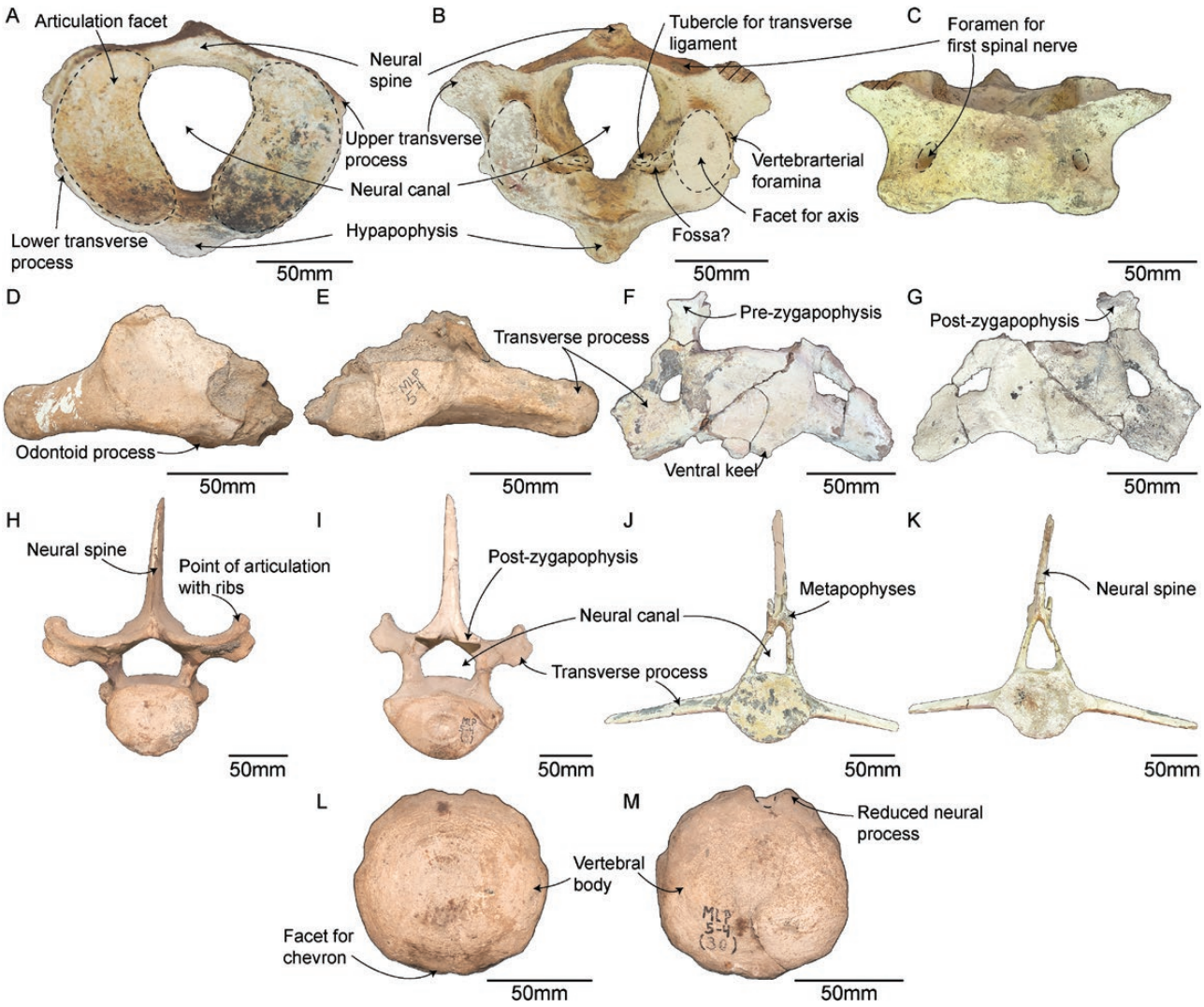

Figure 9. Vertebrae of *Phoberodon arctirostris*. A–C, F, G, J, K, MPEF-PV 10883. D, E, H, I, L, M, MLP 5-3. Depicted are the atlas (A–C), axis (D, E), cervical (F, G), thoracic (H, I), lumbar (J, K) and caudal (L, M) vertebrae. Anterior (A, D, F, H, J, L), posterior (B, E, G, I, K, M) and dorsal (C) views. The position of the cervical, thoracic, lumbar and caudal vertebrae is unknown. Dashed lines indicate specific structures, and hatched outlines show broken areas.

Other cervical vertebrae (Fig. 9): These three vertebrae have a short and wide vertebral body, anteroposteriorly compressed and of oval shape (Supporting Information, Appendix S6). The vertebrae are not fused, as in *Otekaikea* spp. They all have ankylosed epiphyses and a ventral keel. Based on partial preservation, it is inferred that the transverse processes were robust and oriented laterally and that the pre- and postzygapophyses were fully developed.

Thoracic vertebrae (Fig. 9): They all have fused epiphyses, except two in MLP 5-3. The vertebral bodies are rounded in profile, usually wider than high, short, and it is inferred that length increased in a posterior direction (Supporting Information, Appendix S6), similar to *Otekaikea* spp., *S. calvertensis*, *I. vertizi* and *M. ukupachai*. The inferred anterior vertebrae have two points of contact with the ribs (diapophysis and parapophysis), with the parapophysis the biggest. Other vertebrae have only one point of contact with the rib. Transverse processes are either oriented laterally (i.e. perpendicular to the sagittal axis) or slightly posteriorly; they are all thin but have a robust distal end. The preserved neural spines are high (but higher in *A. tokarahi*), thin and oriented almost vertically or posteriorly, with a groove on the posterior surface. The pre- and postzygapophyses are present, as in *S. calvertensis*, *Otekaikea* spp. and *A. tokarahi*; the

former is usually more developed than the latter, and it is inferred that it had a more dorsal position in the most posterior thoracic vertebrae. The neural canal is wide and high.

Lumbar vertebrae (Fig. 9): All vertebrae have rounded vertebral bodies, wider than high, with little variation in their length (Supporting Information, Appendix S6). Ventrally, there is a keel on the centre of each centrum, as in *I. vertizi* and *M. ukupachai*; and dorsally, the neural canal is triangular in shape, as in *S. calvertensis*. The transverse processes are thin and long (whereas they are wider and shorter in *M. ukupachai*) and are oriented perpendicular to the sagittal axis or anteriorly, similar to *O. huata*; they are also more ventrally inclined in anterior view. For the inferred most posterior lumbar vertebrae, the transverse processes shorten. Metapophyses are located dorsally on the anterior margin of the neural canal, and closer to each other on the inferred most posterior lumbar vertebrae, similar to *S. calvertensis*.

Caudal vertebrae (Fig. 9): The inferred most anterior caudal vertebrae have rounded vertebral bodies, higher than wide, whereas the inferred most posterior caudal vertebrae have dorsoventrally and anteroposteriorly compressed bodies (Supporting Information, Appendix S6). The vertebral bodies are similar in *I. vertizi* and *M. ukupachai*. The neural process is short and thin, as are the transverse processes. Metapophyses are still present on the inferred most anterior caudal vertebrae; they are strongly developed and separated from each other, in contrast to the lumbar vertebrae. Some vertebrae have the corresponding dorsal and/or ventral foramen of the vertebrarterial canal, on the lateral side of the vertebral bodies at about the point of insertion of the transverse process, and variably developed articular facets for the chevron bone, similar to *I. vertizi* and *M. ukupachai.*

Ribs (Fig. 10): The ribs preserved are mainly fragmentary. The double-headed ribs are flat, with an angle readily seen and with a weak ridge. The shaft has a flat and slightly swollen surface. The monoccipital ribs have a very flat capitulum and bodies.

Sternum (Fig. 10): Only a partial sternum from MLP 5-3 is preserved. It is presumed to belong to the most anterior portion of this bone (manubrium); it is the widest part of the sternum. No indication of a point of contact with a rib could be recognized. It has an overall squared outline and it does not have any ventral projections, as in *Inia geoffrensis* Blainville, 1817. It has a similar profile to the sternum of *P. davidis* and it is shorter than in *I. vertizi*.

Scapula (Fig. 10): The scapula is fan shaped (Table 3). In life, the scapula was probably oriented with the glenoid cavity ventrally and the suprascapular border dorsally, as assumed in this description. In lateral view, the supraspinous fossa is markedly wider than the infraspinous fossa; the latter fossa is slightly larger than in *Otekaikea* spp. and *A. tokarahi*, and narrower than *P. davidis*. Distally on the infraspinous fossa, there is a strong depression. The spine is distinct, dorsoventrally oriented and does not reach the dorsal margin of the scapular blade. The anterior and posterior borders of the scapula are concave. The acromion projects from the lateral side of the anterior portion of the scapula, not from the anterior edge as it does in *P. gangetica*. It is well developed, longer anteroposteriorly than wider dorsoventrally (Table 3) and thin, with a round anterior edge; it is similar in shape to *Otekaikea* spp. and *P. davidis*. It is oriented perpendicularly to the axis of the scapular spine and parallel to the coracoid process. In an anterior view, the acromion is distinctly curved, resulting in a convex lateral surface and a concave medial surface, similar to *O. huata* and *P. davidis*. The coracoid process is finger like in shape and anteriorly oriented, similar to *A. tokarahi* and more developed than in *P. davidis*. It is longer anteroposteriorly than wider dorsoventrally, and thick (Table 3). It projects from the anterior border of the glenoid cavity. Distally, the glenoid cavity is elliptical and deeply concave (Table 3).

Humerus (Fig. 10): It is long, transversely flattened and with a prominent humeral head (Table 3). The shaft of the humerus has a rectangular profile, with no distinct narrowing, similar to *O. huata*. In posterior view, the medial margin of the humerus is sigmoid. The head is hemispherical and well developed, exposed laterally. Contrary to *P. gangetica* and similar to *M. ukupachai*, the humerus of *P. arctirostris* has distinct greater and lesser tubercles. The greater tubercle is medial to the head and has more gentle edges than the lesser tubercle, which is weakly developed. The lesser tubercle is more developed in *M. ukupachai*. The greater tubercle is the point of insertion for the supraspinatus muscle and the lesser tubercle for the subscapularis. Both tubercles are separated by the intertubercular groove (which is absent in *O. huata*), and the humeral head is separated from the shaft by a shallow neck. On the lateral aspect of the humerus is the area of insertion of the deltoideus muscle (smaller than in *O. huata*), and distal to the head of the humerus is a rounded outline fossa for insertion of the infraspinatus muscle; the latter fossa is similar to *O. huata* and smaller than in *M. ukupachai*. Anterior to the fossa for the infraspinatus is a concave surface, probably where the brachiocephalicus muscle inserted. On the medial aspect of the humerus, there is a small fossa near the posterior margin, probably for the insertion of the teres major muscle. Immediately distal, a rough surface that extends along the width

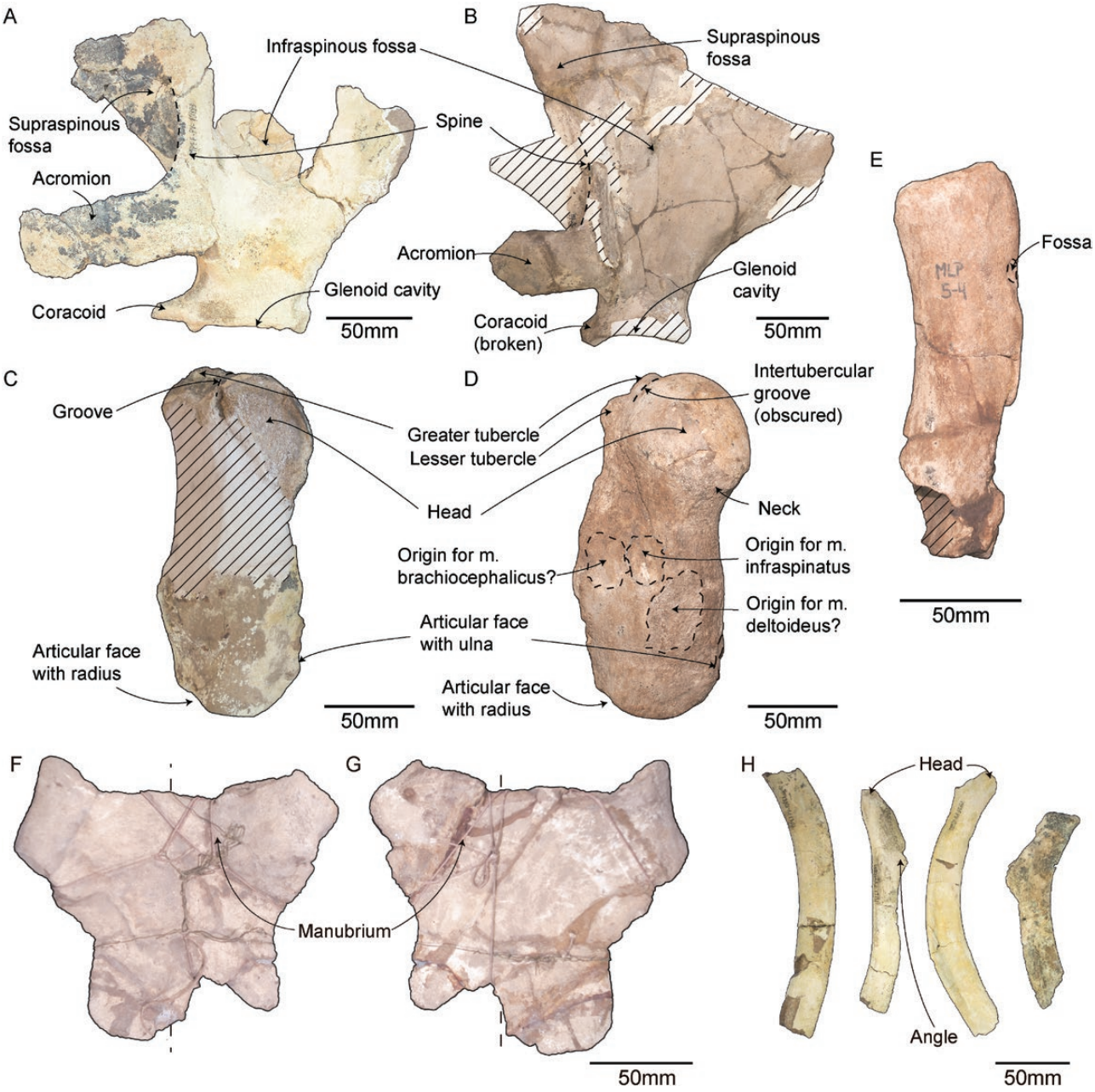

Figure 10. Postcranial elements of *Phoberodon arctirostris*. A, C, H, MPEF-PV 10883. B, D, E, MLP 5-4 (holotype). F–G, MLP 5-3. Scapula (A, B), humerus (C, D), radius (E) (all in lateral view), sternum in dorsal (F) and ventral (G) views, and ribs in lateral view (H).

of the humerus could correspond to the point of insertion of the flexor digitorium. In lateral view, the distal margin of the humerus forms a V-shaped profile. Distally, the articular surfaces for the ulna and radius are smooth, with a concave depression on their centre, separated by a distinct ridge, as in *O. huata*. The articular surface for the ulna extends onto the posterior angle of the humerus. It has a distinct dorsal ridge, thicker laterally, and it is deeply excavated for the olecranon, forming an inverted U shape in profile. There is a groove on the lateral side of this articular surface in MPEF-PV 10883.

Radius (Fig. 10): The radius is dorsoventrally long and anteroposteriorly short (Table 3), longer than in *O. huata* and *P. gangetica*, narrower than in *M. ukupachai*. Both the anterior and the posterior margins are curved, and the shaft narrows

Table 1. Measurements of the skull and mandible of *Phoberodon arctirostris* (in millimetres)

Skull	MLP 5-4 (holotype)	MLP 5-3	MPEF-PV 10883
Total length, from the most anterior point to the posterior margin of condyles	1200	830+	1230+
Length of rostrum	710	565+	770+
Width of rostrum at base	185	200	154.2+
Width of rostrum at half its length	85	75.4	83.2+
Width of premaxillae at a line across posterior limit of antorbital notches	100.4	93.3	84.4?
Greatest length of right nasal	35.7	–	42.3
Greatest width of right nasal	38.4	–	31.1
Distance from tip of rostrum to external nares	800	694.5+	840+
Greatest width of external nares	53.2	56.8	56.0
Anteroposterior length of left antorbital notch	17	12.7?	11.51*
Lateromedial width of left antorbital notch	9.6	2.2?	6*
Length of left premaxillary foramen	17.2	27.6	15
Width of left premaxillary foramen	6.7	6.4	6.9
Length of right premaxillary foramen	20.5	24.5	17.9
Width of right premaxillary foramen	7.3	6.1	5.8
Length of left premaxillary sac fossa	147.7	138.4	117.3*
Width of left premaxillary sac fossa	52.6	22.6	50.6*
Length of right premaxillary sac fossa	128.3	145	98
Width of right premaxillary sac fossa	45.4	39.2	50
Length of right zygomatic process	134.9	104.1	107.2
Width of right zygomatic process	41.6	26.1	35.4
Greatest width of premaxillae	130	117.5	96.6+
Greatest preorbital width at level of preorbital process	263.4	257.2+	189.3+
Greatest postorbital width at level of postorbital process	340	291.2+	208.4+
Length of left orbit, from apex of preorbital process to apex of postorbital process	103.4	101	94.5
Greatest length of right frontal	40.3	–	16.1
Greatest width of right frontal	30.6	–	51.6
Length of upper left tooth row	590	530+	610+
Number of teeth, upper right	15	13+	15
Number of teeth, upper left	15	13+	8+
Mandible			
Greatest length of left ramus	890+	741*	308+
Number of teeth, lower right	13	13	–
Number of teeth, lower left	13	9+	–
Length of lower left tooth row	560	419*	–
Length of left mandibular fossa	60+	186.1*	–
Length of mandibular symphysis	370?	173.8	–
Height of left condyloid process	–	41.6*	–
Width of left condyloid process	–	36.4*	–

Measurements follow Perrin (1975). Symbols: *, measurement from the opposite side; +, nearly complete; ?, uncertainty in the measurement taken.

distally as in *O. huata*, whereas it remains wide in *P. gangetica*. The most distal portion was not preserved completely. The proximal portion has a small and weakly concave articular surface for the humerus. Proximally, the posterior margin has a shallow but distinct fossa.

Comments on trace fossils

Two types of trace fossils were found on some ribs of MPEF-PV 10883. One type consists of parallel linear scrapes, 4–7 mm in length, ~1–3 mm apart and 1 mm wide, slightly curved in the middle; they appear on the body of the ribs. They possibly represent biting traces of a vertebrate, possibly a shark or a small teleost

Table 2. Measurements of teeth and diastema of *Phoberodon arctirostris* (in mm). Symbols: +=nearly complete; ?=uncertainty in the measurement taken

	Measurements (in mm)						
Tooth number	MLP 5-4 (Holotype)			MLP 5-3	MPEF-PV 10883		
	Length	Height	Width	Length	Length	Height	Width
1	12	28	9	–	–	–	–
2	10	19	7	–	–	–	–
3	11	22	9	–	14	24+	11
4	12	20	10	–	15	18+	12
5	11	20	10	–	16	25+	13
6	12	25	9	–	17	19+	13
7	–	–	–	–	19	24+	12
8	13+	14+	9+	–	18	17+	12
9	16	25	10	–	19	12+	13
10	15	23	10	–	23	29+	13
11	18	20+	9	–	22	9+	13
12	10+	18+	?	–	–	–	–
13	–	–	–	–	–	–	–
14	20	17	8	–	26	27+	13
15	17	18	8	–	24	29+	14
Diastema							
1 – 2	19			18	8		
2 – 3	24			20	12		
3 – 4	25			19	24		
4 – 5	24			21	30		
5 – 6	31			23	24		
6 – 7	32?			24	25		
7 – 8	25?			20	24?		
8 – 9	33			18	25		
9 – 10	26			14	24		
10 – 11	28			10	21		
11 – 12	27			10	24?		
12 – 13	14			–	21		
13 – 14	9			–	13		
14 – 15	8			–	–		

(Noriega *et al.*, 2007). A second type appears near the margin of the distal portion of the ribs, consisting of several small and finely sculptured radiating traces, 1–2 mm long. They are tentatively assigned to the gastropod ichnogenus *Radulichnus* (Cione *et al.*, 2010). More evidence of trace fossils on cetaceans and other vertebrate remains from the Gaiman Formation are currently under study (J.I.C.). No trace fossils were found on the holotype and MLP 5-3, because they are covered with glue from antique preparation techniques.

Phylogenetic analysis

In the present study, two different cladistic analyses were performed: equal weights and implied weights. Below are the results and discussion of both analyses.

Under equal weights, the analysis recovered 164 trees of 1912 steps (consistency index = 0.23; retention index = 0.64; Fig. 11). The strict consensus shows *P. arctirostris* forming a clade with the undescribed OU 21798, supported by one ambiguous synapomorphy, rostral constriction anterior to maxillary flange (character 9), and four unambiguous synapomorphies: frontal forming dorsolateral margin of ventral infraorbital foramina (character 45); postorbital process of frontal oriented ventrally (character 48); straight margin of premaxilla posterior to premaxillary foramina (character 57); and presence of a deep neck muscle fossa on zygomatic process of squamosal (character 114). *Phoberodon arctirostris* presents 12 autapomorphies: long rostrum (character 1); wide premaxilla at mid-rostrum (character 11); unfused maxilla and premaxilla

Table 3. Measurements of the postcranial elemnts of *Phoberodon arctirostris* (in mm). Measurements follow Perrin (1975) and Buchholtz *et al.* (2005). Only the greatest dimension for each type of vertebrae are indicated. For the full list of measurements, see Appendix S1. Symbols: +=nearly complete; ?=uncertainty in the measurement taken

	Measurements (in mm)		
VERTEBRAE	MLP 5-4 (Holotype)	MLP 5-3	MPEF-PV 10883
Atlas			
Greatest height	112.8	–	114.9
Greatest width	139.4	–	149.1+
Axis			
Greatest height	65.6+	–	77.5+
Greatest width	126.2+	–	77.1+
Cervical			
Greatest height	95.3+	70+	92.3+
Greatest width	111.2+	99.5+	149.3+
Greatest length of centrum	25.9	26.9	23.7
Thoracic			
Greatest height	160.5+	170.8+	231.4+
Greatest width	167.6+	115.7+	133+
Greatest length of centrum	51	58.5	51.7
Lumbar			
Greatest height	216.9+	182.3+	226.6+
Greatest width	183.8+	214.7+	296.8+
Greatest length of centrum	86.6	82.4	96.1
Caudal			
Greatest height	137.3+	196.1+	189.1+
Greatest width	104.4	152.9+	84.8+
Greatest length of centrum	80.9	80.8	72.5+
SCAPULA (LEFT)			
Height, from the posterior margin of glenoid fossa to coracoventral angle	274.6	–	201.1+
Length, from the posterior margin of the glenoid fossa to glenovertberal angle	191.2+	–	136+
Greatest length of coracoid process, from anterior margin of glenoid fossa	11.3	–	19.5
Greatest width of coracoid process	17.6	–	11
Greatest length of acromion process	11.3+	–	99.7+
Length of glenoid fossa	70.5	–	55.2
Width of glenoid fossa	49.9	–	37.9
HUMERUS			
Greatest length of humerus	176.3	–	187.7+
Greatest width of humerus	73.9	–	69.4+
RADIUS			
Greatest length of radius	157.6+	–	–
Greatest width of radius	50.9	–	–

along rostrum (character 15); maxilla forms the posterior wall of the antorbital notch (character 16); presence of a longitudinal groove on underside of mandibles (character 33); straight mandible (character 34); absence of an antorbital process of maxilla (character 36); anteromedially oriented orbit (character 37); presence of a dorsal infraorbital foramina near posterior extremity of premaxilla (character 60); convex ventral edge of zygomatic process of squamosal (character 116); expanded tympanosquamosal recess on squamosal (character 149); and moderately concave posterior sinus fossa of exoccipital (character 166). Crownward to this clade are *P. davidis* then *S. calvertensis*, followed by Platanistoidea (i.e. ZMT-73 + *A. talen* + *A. tokarahi* +

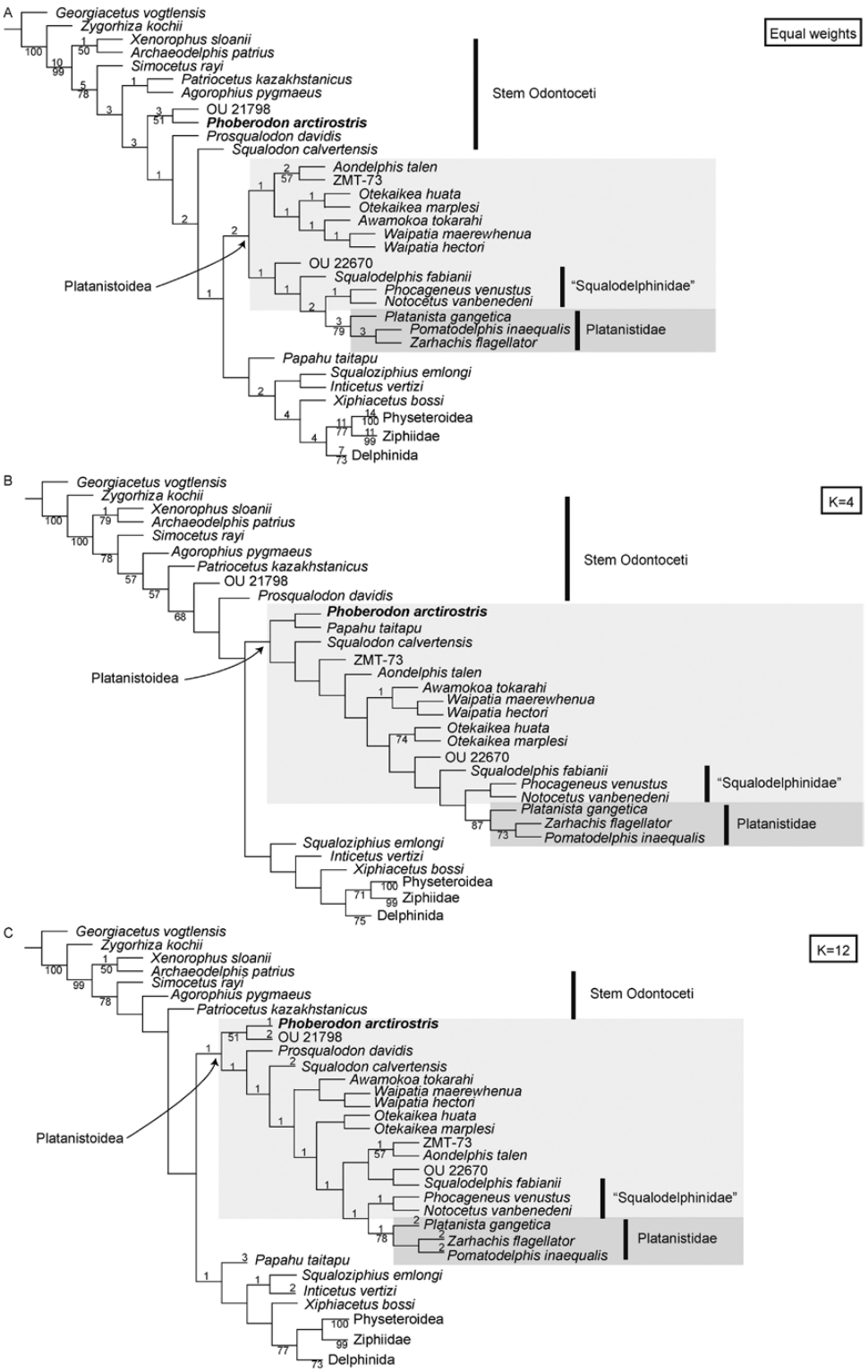

Figure 11. Phylogenetic hypotheses obtained for the position and relationships of *Phoberodon arctirostris*. A–C, strict consensus tree of analysis under equal weights (A) and implied weights analyses with $K = 4$ (B) and $K = 12$ (C). Numbers above branches indicate Bremer support, and numbers below branches indicate jackknife support using $P = 0.30$ and 1000 pseudoreplicates. Light grey, stem Platanistoidea; dark grey, crown Platanistoidea. For ease of illustration, clade Delphinida *sensu* Geisler *et al.* (2011) was collapsed.

Otekaikea spp. + *Waipatia* spp. + OU 22670 + 'Squalodelphinidae' + Platanistidae). For Platanistoidea, we will refer to crown Platanistoidea (Platanistidae, i.e. *P. gangetica* + *P. inaequalis* + *Z. flagellator*) and stem Platanistoidea (i.e. ZMT-73 + *A. talen* + *A. tokarahi* + *Otekaikea* spp. + *Waipatia* spp. + OU 22670 + 'Squalodelphinidae'). Clade Platanistoidea is supported by seven ambiguous synapomorphies: short crown of heterodont teeth (character 23; unknown in *A. talen*, ZMT-73, *Otekaikea* spp., *A. tokarahi*, *W. hectori*, OU 22670, *Phocageneus venustus* Leidy, 1869 and Platanistidae); wide premaxilla at base of rostrum (character 53; unknown in *A. talen*, ZMT-73, *O. huata*, *A. tokarahi*, *W. hectori*, OU 22670, *P. venustus* and *P. gangetica*); nuchal crest at same level as nasal and frontal (character 101; except *S. fabianii* and *P. inaequalis* and unknown in *A. talen*, ZMT-73, *A. tokarahi*, *W. hectori*, *P. venustus*, *N. vanbenedeni* and *P. gangetica*); shallow posterior portion of periotic fossa (character 155; except in *N. vanbenedeni* and Platanistidae and unknown in *A. tokarahi*, OU 22670 and *P. venustus*); anteroposterior ridge on dorsal side of anterior process and body of periotic (character 174; except ZMT-73 and unknown in *W. hectori*, OU 22670 and *S. fabianii*); thin pars cochlearis of periotic (character 193; except *A. tokarahi* and *W. maerewhenua* and unknown in *W. hectori*, OU 22670, *S. fabianii*, *P. inaequalis* and *Z. flagellator*); subrectangular cochlear aqueduct on periotic (character 194; except *A. talen*, *P. venustus* and *N. vanbenedeni* and unknown in *W. hectori*, OU 22670, *S. fabianii*, *P. inaequalis* and *Z. flagellator*); and concave ventral surface of posterior process of periotic (character 201; unknown in ZMT-73, *W. hectori*, OU 22670, *S. fabianii* and *Z. flagellator*). ZMT-73 and *A. talen* form a clade, always included within stem Platanistoidea. Family 'Squalodelphinidae' is recovered as a paraphyletic group, comprising *S. fabianii*, *N. vanbenedeni* and *P. venustus*. In contrast, *I. vertizi* is recovered as closely related to *Squaloziphius emlongi* Muizon, 1991, and not within platanistoids or stem odontocetes. Finally, the IterPCR analysis did not identify *P. arctirostris* as an unstable taxon (Supporting Information, Appendix S4).

For the analysis under implied weight, several *K* values were tested (see 'Material and methods' section), and we will discuss only the MPTs of *K* = 4 and *K* = 12 because the topology is different between them and the strict consensus tree of the analysis under equal weights.

With *K* = 4, one MPT was recovered (fit = 126.90, 1944 steps; Fig. 11). OU 21798 is the earliest diverging taxon, followed by *P. davidis*. Next is clade Platanistoidea, with *P. arctirostris* closely related to *Papahu taitapu* Aguirre-Fernández & Fordyce, 2014. The latter are supported by three unambiguous synapomorphies: anteromedially oriented orbit (character 37); shallow neck muscle fossa on zygomatic process of squamosal (character 114); and expanded tympanosquamosal recess (character 149); and by one ambiguous synapomorphy: dorsolateral edge of ventral infraorbital foramina formed by frontal (character 45; unknown in *P. taitapu*). *Phoberodon arctirostris* has 15 autapomorphies, sharing only five with the previous analysis (characters 15, 16, 36, 60 and 116). The other autapomorphies are: rostral constriction anterior to maxillary flange (character 9); wide rostrum at base (character 13); lacrimal restricted below the supraorbital process (character 39); pointed postorbital process of frontal (character 49); premaxillary foramen anterior to antorbital notch (character 55); straight lateral margin of right premaxilla posterior to the premaxillary foramen (character 57); absence of a maxillary crest (character 66); absence of a maxillary intrusion (character 71); absence of a premaxillary crest (character 72); and posterior-most portion of alisphenoid–squamosal suture anterior to foramen ovale (character 151). Following these taxa are: *S. calvertensis* and clade Platanistoidea, comprising the same species as the analyses under equal weights (see above); the latter clade is supported by three ambiguous synapomorphies (characters 22, 86 and 247). Finally, *P. davidis* remains as a member of stem Odontoceti (Fig. 11).

With *K* = 12, only one MPT was recovered (fit = 72.76, 1917 steps), and the topology is very similar to *K* = 4 (Fig. 11), except that now *P. davidis* is recovered within stem Platanistoidea. Thus, this clade is now more inclusive than the previous analyses. Here, *P. arctirostris* forms a clade with OU 21798, like the analysis under equal weights, supported by eight synapomorphies (characters 9, 13, 45, 49, 57, 66, 90 and 114). Also, *P. arctirostris* presents the same synapomorphies as the analysis under equal weights, with the addition of another one: wide rostrum (character 12). Clade Platanistoidea is supported by five synapomorphies (characters 76, 86, 175, 178 and 196), and the clade *A. talen* + ZMT-73 is now closely related to *S. fabianii* and OU 22670.

Implied weights has been pointed out as dealing better with homoplasy for morphological data sets (e.g. Goloboff *et al.*, 2008, 2017), but some authors have also raised the concern that this method has some inconsistencies and insufficient accuracy (e.g. Congreve & Lamsdell, 2016; Puttick *et al.*, 2017). For the present study, we will base our discussion on the equal weights phylogenetic hypothesis.

DISCUSSION

PHYLOGENETIC RELATIONSHIPS

Superfamily Platanistoidea has a long and highly variable taxonomic history (e.g. Muizon 1987, 1994;

Barnes *et al.*, 2010; Lambert *et al.*, 2014, 2018; Tanaka & Fordyce, 2014, 2015a,b, 2016, 2017; Boersma & Pyenson, 2016; Kimura & Barnes, 2016; Boersma *et al.*, 2017), and there is still a need for modern revisions and species description, in order to comprehend the diversity and evolutionary history of this enigmatic group. In addition, family Squalodontidae has also been proposed as part of Platanistoidea (e.g. Muizon, 1987, 1991, 1994; Fordyce, 1994) but never tested in a phylogenetic analysis. Squalodontids nominally include several genera, some of them based on fragmentary material, that have not been revised or analysed recently, such as *Squalodon*, *Eosqualodon*, *Patriocetus*, *Prosqualodon*, *Sulakocetus* and *Neosqualodon* (e.g. Kellogg, 1923; Rothausen, 1968; Fordyce, 1994; Muizon, 1991; Fordyce & Muizon, 2001). The phylogenetic relationships of *P. arctirostris* have been contentious, with some authors placing this taxon within Squalodontidae (Cabrera, 1926; Simpson, 1945; Fordyce, 1994) or in a close relationship with *W. maerewhenua* (Cozzuol, 1996) or even within Platanistoidea (Muizon 1987, 1991, 1994).

The results of our analyses recovered *P. arctirostris* as a stem Odontoceti, more closely related to an undescribed New Zealand specimen (OU 21798) than to *P. davidis*, *S. calvertensis* and Platanistoidea, which contradicts previous assessments of the phylogenetic affinities of this taxon. *Phoberodon arctirostris* shares with OU 21798 some plesiomorphic characteristics, such as the following: the frontal forming the dorsolateral margin of the ventral infraorbital foramen; a low vertex, with wide nasals and the presence of a narial process of the frontal; heterodont dentition, teeth with a long crown and cheek teeth with accessory denticles; wide and inflated premaxillae at the rostrum that do not contact each other; wide rostrum at its base; reduced number of teeth in mandible; and absence of a maxillary crest and maxillary intrusion.

Some of the plesiomorphic skull characteristics of *P. arctirostris* have historically related it to *S. calvertensis* and even a member of Squalodontidae (e.g. Kellogg, 1923, 1928; Muizon, 1991; Fordyce, 1994; Barnes *et al.*, 2010); for example, a long skull, low vertex and triangular cheek teeth, with rugose enamel (e.g. Kellogg, 1923; Fordyce, 1994). However, *P. arctirostris* is distinct from *S. calvertensis* and *P. davidis* in having, for example, a transversely inflated premaxilla at the rostrum, nasals with a concave posterior margin and presence of a supraspinous fossa of the scapula (for further detail, see emended diagnosis). *Phoberodon arctirostris* tooth morphology has also been considered as squalodontid like (Kellogg, 1928); however, many of these characters are plesiomorphies also shared with other heterodont odontocetes and require testing in phylogenetic analyses.

Phoberodon arctirostris is also distinct from *Eosqualodon latirostris* Capellini, 1903 in the absence of an intertemporal constriction, supraoccipital less expanded anteriorly, wider maxilla at the rostrum and more expanded laterally at the orbital region, smaller temporal fossa, external nares more posteriorly placed, lower vertex and more robust zygomatic process of the squamosal. In contrast, both species share a long rostrum, the presence of subparallel ridges on the enamel of anterior cheek teeth and the presence of double-rooted posterior cheek teeth with accessory denticles (Capellini, 1903). It should be noted that the earbone morphology of *E. latirostris* remains unknown, as in *P. arctirostris*.

Also, Cozzuol (1996) proposed a close relationship between *P. arctirostris* and *W. maerewhenua*, and even the inclusion of the species within Waipatiidae, based on shared characteristics of the basicranial region (however, the author did not specify which characteristics); our results did not recover such relationship.

The presence of plesiomorphic skull characteristics might be strongly influencing the basal position of *P. arctirostris* recovered in the present analysis. However, under implied weights *P. arctirostris* was recovered as an early-diverging member of Platanistoidea, forming a clade with OU 21798 or with *P. taitapu* (Fig. 11). This position might reflect the presence of more derived characters in *P. arctirostris*, such as: long maxilla in rostrum and forming posterior wall of antorbital notch, presence of longitudinal groove on underside of mandible, frontal forming dorsolateral edge of ventral infraorbital foramina, ventrally oriented postorbital process, premaxillary foramen posterior to antorbital notch, presence of posterior dorsal infraorbital foramen, absence of maxillary intrusion, shallow premaxillary cleft, convex ventral edge of zygomatic process, very large tympanosquamosal recess and moderately concave posterior sinus fossa; and thus represent an intermediate morphology between stem odontocetes (such as *S. calvertensis* and *P. davidis*) and more crownward platanistoids.

Our results suggest that the position of *P. arctirostris* is still controversial. This could be attributable, in part, to the lack of tympanoperiotic or basicranial information. Earbone characters have a strong phylogenetic signal (e.g. Tsai & Fordyce, 2016; Tanaka & Fordyce, 2017); therefore, the future recovery and description of these bones might influence the phylogenetic position of this species. It is desirable that new specimens with earbones are included in future analyses to test the phylogenetic position of *P. arctirostris* further.

Unlike other authors (e.g. Kellogg, 1923, 1928; Rothausen, 1968; Muizon, 1991; Fordyce, 1994), our

analyses did not recover Squalodontidae as a clade. Furthermore, the analyses did not recover *P. davidis* or *S. calvertensis* as members of Platanistoidea (except under implied weights), unlike Muizon (1994), Barnes (2006), Barnes *et al.* (2010) and Lambert *et al.* (2018). Instead, these taxa were recovered as stem odontocetes but immediately basal to Platanistoidea and the remaining crown Odontoceti.

The diagnosis of Squalodontidae has been based on the following: bilaterally flattened posterior cheek teeth with a triangular crown, rugose enamel and presence of accessory denticles (Kellogg, 1923; Rothausen, 1968; Keyes, 1973; Fordyce, 1994; Dooley, 2003); anterior cheek teeth with small and widely separated denticles on the anterior and posterior keel (Fordyce, 1994); enlarged incisors that protrude anteriorly (Muizon, 1991); heterodonty and polydonty (Rothausen, 1968); long skull, CBL > 700 mm (Fordyce, 1994); upturned rostrum and mandible (Dooley, 1998); narrow and deep mesorostral groove, resulting in a posteriorly deep rostrum (Fordyce, 1994); long rostrum with wide apex (Kellogg, 1928; Muizon, 1991); the premaxilla bears alveoli (Rothausen, 1968) with incisors that are circular and have straight serrated edges (Dooley, 1998); first incisor lies dorsal to second one (Dooley, 1998); reduction of lateral lamina of pterygoid (Muizon, 1991; Dooley, 1998); posteriorly placed nares (Rothausen, 1968); low vertex, with shortened nasals and absence or reduced presence of parietals (Kellogg, 1923, 1928; Rothausen, 1968; Dooley, 2003); presence of crescentic foramina on nasal passage (Kellogg, 1928); maxilla contacts posteriorly with supraoccipital and covers most of the frontal laterally (Kellogg, 1928; Rothausen, 1968; Dooley, 2003); reduced or lacking intertemporal constriction (Rothausen, 1968); and oval humeral head (Dooley, 1998). Some earbone characteristics have been proposed as diagnostic of the family; for example, subcylindrical anterior process with prominent tubercle on apex of periotic, narrow and dorsoventrally deep dorsal surface of periotic, elongated posterior bullar facet of periotic and spongy posterior process of tympanic bulla (Fordyce, 1994; Dooley, 1998, 2003). Most of the characteristics were not phylogenetically tested, some of them represent plesiomorphies, and there is scope to identify more diagnostic characteristics for the group. In addition, many of the squalodontid taxa have been described from fragmentary specimens of questionable allocation, which has hampered a better resolution of the relationships and contents of this family (Fordyce & Muizon, 2001). Even though there have been rich advances in recent years in the study of platanistoids (e.g. Tanaka & Fordyce, 2014, 2015a,b, 2016, 2017; Viglino *et al.*, 2018), more squalodontid taxa need phylogenetic analysis to clarify the definition and contents of this family (e.g. Kellogg, 1923; Fordyce, 1994; Fordyce & Muizon, 2001).

Our results consistently recovered a speciose clade Platanistoidea, although with some variation in the content (Fig. 11). Given that crown Platanistoidea is always composed of family Platanistidae, we now focus on the varying contents of the members of stem Platanistoidea. The taxa that were consistently recovered within stem Platanistoidea are ZMT-73 + *A. talen* + *Waipatia* spp. + *Otekaikea* spp. + *A. tokarahi* + OU 22670 + 'Squalodelphinidae', in agreement with recent studies (e.g. Tanaka & Fordyce, 2014, 2015a,b, 2016; Boersma & Pyenson, 2016) but in contrast to others (e.g. Lambert *et al.*, 2014, 2018; Boersma *et al.*, 2017). One of the synapomorphies (character 174) agrees with Tanaka & Fordyce (2014) and Boersma & Pyenson (2016). However, we did not recover any of the synapomorphies of Tanaka & Fordyce (2014, 2016, 2017). Unlike Boersma *et al.* (2017) and Lambert *et al.* (2014), we recovered a paraphyletic but fully resolved 'Squalodelphinidae' family (Tanaka & Fordyce, 2014, 2015a,b, 2016, 2017; Boersma & Pyenson, 2016). Currently, one of the authors (M.V.) is conducting a revision of *N. vanbenedeni*, which should help to clarify the contents and relationships of this family.

This is the first modern anatomical description and phylogenetic analysis of *P. arctirostris*, a long-neglected early Miocene species from Patagonia. Our results suggest that during this epoch, archaic odontocete forms (e.g. *P. arctirostris*) plus both archaic (e.g. *A. talen*; Viglino *et al.*, 2018) and more crownward platanistoids (e.g. *N. vanbenedeni*) cohabited in the southwestern Atlantic. Given that their skull anatomy is distinct, especially involving the feeding apparatus, there was probably no ecological overlap. Stratigraphically focused fieldwork should elucidate the diversity and palaeoecological patterns of early Miocene odontocete communities in Patagonia.

Scapular morphology

Muizon (1987, 1991, 1994) suggested as synapomorphies of superfamily Platanistoidea the great reduction of the coracoid process (also suggested by Kimura & Barnes, 2016) and the great reduction or loss of the supraspinous fossa, with the acromion located on the anterior edge of the scapula. Muizon, based on Cabrera's illustration, stated that *P. arctirostris* had this condition and could therefore be included within the superfamily. Based on our description, *P. arctirostris* presents a well-developed and distally expanded acromion (like *O. huata* and *S. calvertensis*), and it is located on the lateral side of the anterior margin of the scapula, as suggested by Cozzuol & Humbert-Lan (1989). *Phoberodon arctirostris* has an acromion

directed horizontally when the glenoid fossa is oriented ventrally (character 248; Fig. 10), an autapomorphic condition among stem Odontoceti and shared only with more crownward Delphinida according to our phylogenetic analysis. A distinct supraspinous fossa is present (contrary to Muizon, 1987, 1991, 1994), similar to *Otekaikea* spp., *A. tokarahi*, *P. davidis* and *Ninjadelphis ujiharai* Kimura & Barnes, 2016 (Kimura & Barnes, 2016) and different from *P. gangetica*, in which this fossa is absent. Also, as stated by Muizon (1994) and Cabrera (1926), the coracoid process of *P. arctirostris* is reduced, as in *O. huata*, *A. tokarahi* and an unnamed waipatiid (Fitzgerald, 2016), and it originates on the anterior edge of the glenoid fossa.

As has been pointed out, some previous analyses have suggested some scapular characters as diagnostic of the entire superfamily. However, neither previous (e.g. Tanaka & Fordyce, 2014, 2015a, 2016; Boersma & Pyenson, 2016; Boersma *et al.*, 2017) nor the present phylogenetic analysis recovered scapular characteristics as synapomorphies of Platanistoidea (except under implied weights with $K = 4$; see 'Phylogenetic analysis' results). Regarding the loss of the supraspinous fossa and position of the acromion process, our analysis suggests that it could be a shared morphology between some stem odontocetes (e.g. *P. davidis* and *S. calvertensis*), some of the most crownward platanistoid families (i.e. Platanistidae and 'Squalodelphinidae') and one delphinid species (*Sotalia fluviatilis* Gervais & Deville in Gervais, 1853; see matrix in Supporting Information, Appendix S3 and Fettuccia, 2010). Several fossil taxa do not include a preserved scapula, and together with the complex morphological variability observed on this bone, this might explain the low phylogenetic signal of this character (Cozzuol, 1996).

Evolution of body size

Regarding the reconstructed total length of 3.1 m for *P. arctirostris*, it is worth noting that it would represent one of the largest stem odontocetes, similar to *P. davidis* (total length 3.15 m; Flynn, 1948), OU 21798 (total length 3.6 m), *I. vertizi* (total length 3.4 m; Lambert *et al.*, 2018) and *M. ukupachai* (total length 3.5 m; Bianucci *et al.*, 2018). *Phoberodon arctirostris* would appear to be larger than other basal stem Odontoceti, such as *Simocetus rayi* Fordyce, 2002 (total length 2.33 m; Fordyce, 2002) and *Agorophius pygmaeus* Müller, 1849 (total length 2 m; Godfrey *et al.*, 2016). Furthermore, *P. arctirostris* exhibits a greater total length than *S. calvertensis* (total length 2.8 m; Kellogg, 1923), *P. taitapu* (total length 1.9 m; Aguirre-Fernández & Fordyce, 2014) and early-diverging platanistoids (e.g. *O. marplesi*, total length 2.5 m, Tanaka & Fordyce, 2014; *O. huata*, total length 2.6 m, Tanaka & Fordyce, 2015a; *Waipatia marewhenua*, total length 2.4 m, Fordyce, 1994).

The evolution of body size in cetaceans is complex, and it is beyond the scope of this contribution to provide a comprehensive study of this topic. However, among platanistoids and comparable stem taxa, the analysis of body length indicates that the late Oligocene–early Miocene was a time of diverse body sizes among stem odontocetes and platanistoids, showing a trend towards decreasing body size (Bianucci *et al.*, 2018), with the extant representative *P. gangetica* having a total length of 2.6 m for adult females and 2.2 m for adult males (Perrin *et al.*, 2008). This trend among platanistoids is in accordance with the proposed general decrease in body length through time for odontocetes (e.g. Slater *et al.*, 2010).

Furthermore, coeval early Miocene odontocetes in Patagonia were large (e.g. *P. arctirostris*) and medium sized (e.g. *N. vanbenedeni*, *A. talen*; Viglino *et al.*, 2018), further obviating ecological niche overlap (Velez-Juarbe *et al.*, 2012). *Phoberodon arctirostris* would represent a large predator within the early Miocene odontocete Patagonian community, and its large body size might indicate that it was able to consume a larger variety of prey sizes and belonged to higher trophic levels (e.g. Cohen *et al.*, 1993; Woodward *et al.*, 2005).

Conclusions

This is the first modern description and phylogenetic analyses of a long-forgotten odontocete species from the early Miocene of Patagonia, *P. arctirostris*. Anatomical studies indicate that *P. arctirostris* is a large odontocete with a slightly asymmetrical skull. The rostrum is proportionally longer than the cranium, with robust heterodont teeth, anteriorly oriented and procumbent anterior incisors, and a cranium with a low vertex. Tympanoperiotic morphology is unknown. The revision of the scapular morphology of this taxon suggests a lack of the putative platanistoids synapomorphies on this bone as suggested by previous authors. Our results did not recover scapular characters as synapomorphies of Platanistoidea. Furthermore, phylogenetic analyses showed *P. arctirostris* to be closely related to a New Zealand undescribed species (OU 21798) within stem Odontoceti, and only recovered *P. arctirostris* as an early-diverging member of Platanistoidea under implied weights. Thus, the phylogenetic position of *P. arctirostris* is still controversial. The species does not form a clade with either *P. davidis* or *S. calvertensis*, as suggested by previous authors. During the early Miocene in Patagonia, coeval odontocetes were either large (e.g. *P. arctirostris*) or medium sized (e.g. *N. vanbenedeni*, *A. talen*) and represent different morphotypes, including both archaic odontocete forms (e.g. *P. arctirostris*) and archaic (e.g. *A. talen*) and more crownward platanistoids

(e.g. *N. vanbenedeni*). These results might suggest a lack of ecological overlap, because the species occupied different niches, and explain the diversity of odontocetes during this time in Patagonia.

ACKNOWLEDGEMENTS

First of all, we would like to thank the Morrison family, whose tip provided the new specimen used for this study. We thank them for their patience and interest in the study of fossil cetaceans of Patagonia. We thank S. Bessone (IPGP) for specimen preparation, S. Bessone (IPGP) and F. Busker (IPGP) for assistance during fieldwork and M. T. Dozo (IPGP) for permits for access. We thank the following curators for access to the collections under their care: E. Ruigomez (MEF), M. Reguero and A. Scarano (MLP), P. Teta and S. Lucero (MACN), N. Pyenson (USNM), N. B. Simmons (AMNH) and A. van Helden (NMNZ). We would also like to thank Y. Tanaka (Numata Fossil Museum) and D. Perez (MACN) for useful discussions regarding the matrix and phylogenetic analysis. We thank O. Lehmann (UBA) for lending the script used for analysis of multiple implied weights. This contribution used TNT v. 1.5, a program made freely available thanks to a subsidy by the Willi Hennig Society. We would also like to thank D. del Castillo (UBA) for access to their photographs of cetacean specimens revised. We would like to thank the following organizations for financial support: Cetacean Society International (CSI) to M.V. and M.R.B.; Learner-Gray Grant from the American Museum of Natural History (AMNH) to M.R.B.; Sociedad Argentina para el Estudio de Mamíferos (SAREM) to M.V.; Smithsonian Institution (Remington Kellogg Fund) to M.R.B.; Agencia Nacional de Promoción Científica y Tecnológica (grant number PICT 0792) to M.B. and J.I.C.; and an Australian Research Council Linkage Project (grant number LP150100403) to E.M.G.F.

AUTHOR CONTRIBUTIONS

Conceived and designed the experiments: M.V. and M.R.B. Performed the experiments: M.V., M.R.B. and J.I.C. Analysed the data, contributed reagents/materials/analysis tools and wrote the paper: M.V., M.R.B., J.I.C., R.E.F. and E.M.G.F.

REFERENCES

Acosta Hospitaleche C, Castro L, Tambussi C, Scasso RA. 2008. *Palaeospheniscus patagonicus* (Aves, Sphenisciformes): new discoveries from the early Miocene of Argentina. *Journal of Paleontology* **82:** 565–575.

Aguirre-Fernández G, Fordyce RE. 2014. *Papahu taitapu*, gen. et sp. nov., an Early Miocene stem odontocete (Cetacea) from New Zealand. *Journal of Vertebrate Paleontology* **34:** 195–210.

Anderson J. 1878. *Anatomical and zoological researches comprising an account of the zoological results of the two expeditions to Western Yunnan in 1868 and 1875 and a monograph of the two cetacean genera, Platanista and Orcella*. London: B. Quaritch.

Barnes LG. 2006. A phylogenetic analysis of the superfamily Platanistoidea. *Beiträge Zur Paläontologie* **30:** 25–42.

Barnes LG, Kimura T, Godfrey SJ. 2010. The evolutionary history and phylogenetic relationships of the Superfamily Platanistoidea. In: Ruiz-García M, Shostell JM, eds. *Biology, evolution and conservation of river dolphins within South America and Asia*. New York: Nova Science Publishers, 445–488.

Bercovici A, Hadley A, Villanueva-Amadoz U. 2009. Improving depth of field resolution for palynological photomicrography. *Palaeontologia Electronica* **12:** pp.12.2.5T.

Bianucci G, Bosio G, Malinverno E, de Muizon C, Villa IM, Urbina M, Lambert O. 2018. A new large squalodelphinid (Cetacea, Odontoceti) from Peru sheds light on the Early Miocene platanistoid disparity and ecology. *Royal Society Open Science* **5:** 172302.

Boersma AT, McCurry MR, Pyenson ND. 2017. A new fossil dolphin *Dilophodelphis fordycei* provides insight into the evolution of supraorbital crests in Platanistoidea (Mammalia, Cetacea). *Royal Society Open Science* **4:** 170022.

Boersma AT, Pyenson ND. 2016. *Arktocara yakataga*, a new fossil odontocete (Mammalia, Cetacea) from the Oligocene of Alaska and the antiquity of Platanistoidea. *PeerJ* **4:** e2321.

Buchholtz EA, Wolkovich EM, Cleary RJ. 2005. Vertebral osteology and complexity in Lagenorhynchus acutus (Delphinidae) with comparison to other delphinoid genera. *Marine Mammal Science* **21:** 411–428.

Buono MR, Fernández MS, Cozzuol MA, Cuitiño JI, Fitzgerald EMG. 2017. The early Miocene balaenid *Morenocetus parvus* from Patagonia (Argentina) and the evolution of right whales. *PeerJ* **5:** e4148.

Buono MR, Viglino M, Cozzuol MA, Lucero S. 2016. Descifrando la historia evolutiva de los Neoceti (Mammalia: Cetacea): aportes del registro fósil del Neógeno del Atlántico Sudoccidental. *Contribuciones del MACN* **6:** 323–334.

Cabrera A. 1926. Cetáceos fósiles del Museo de La Plata. *Revista del Museo La Plata* **29:** 363–411.

Capellini G. 1903. Avanzi di squalodonte nella arenaria di grumi dei frati. *Memorie della Reale Accademia delle Scienze dell'Istituto di Bologna* **5:** 437–445.

Cione AL, Acosta Hospitaleche C, Pérez LM, Laza JH, César I. 2010. Trace fossils on penguin bones from the Miocene of Chubut, southern Argentina. *Alcheringa: an Australasian Journal of Palaeontology* **34:** 433–454.

Cione AL, Cozzuol MA, Dozo MT, Acosta Hospitaleche C. 2011. Marine vertebrate assemblages in the southwest Atlantic during the Miocene. *Biological Journal of the Linnean Society* **103:** 423–440.

Coddington JA, Scharff N. 1994. Problems with zero-length branches. *Cladistics* **10:** 415–423.

Cohen JE, Pimm SL, Yodzis P, Saldaña J. 1993. Body sizes of animal predators and animal prey in food webs. *Journal of Animal Ecology* **62:** 67–78.

Congreve CR, Lamsdell JC. 2016. Implied weighting and its utility in palaeontological datasets: a study using modelled phylogenetic matrices. *Palaeontology* **59:** 447–462.

Cozzuol MA. 1996. The record of the aquatic mammals in southern South America. *Munchner Geowissenschaftliche Abhandlungen* **30:** 321–342.

Cozzuol MA, Humbert-Lan G. 1989. On the systematic position of the genus *Prosqualodon* Lydekker, 1893, and some comments on the odontocetes family Squalodontidae. *Abstract book of the 5th International Theriological Congress* **1:** 483–484.

Cuitiño JI, Pimentel MM, Santos RV, Scasso RA. 2012. High resolution isotopic ages for the early Miocene "Patagoniense" transgression in Southwest Patagonia: stratigraphic implications. *Journal of South American Earth Sciences* **38:** 110–122.

Cuitiño JI, Scasso RA, Ventura Santos R, Mancini LH. 2015a. Sr ages for the Chenque Formation in the Comodoro Rivadavia region (Golfo San Jorge Basin, Argentina): stratigraphic implications. *Latin American Journal of Sedimentology and Basin Analysis* **22:** 3–12.

Cuitiño JI, Ventura Santos R, Alonso Muruaga PJ, Scasso RA. 2015b. Sr-stratigraphy and sedimentary evolution of early Miocene marine foreland deposits in the northern Austral (Magallanes) Basin, Argentina. *Andean Geology* **42:** 364–385.

Dal Piaz G. 1917. Gli odontoceti del Miocene bellunese Parte terza *Squalodelphis fabianii*. *Memorie dell' Instituto Geologico della R. Universita di Padova* **5:** 3–34.

Dooley AC Jr. 1998. *A review of the North America Squalodontidae (Mammalia, Cetacea)*. Unpublished D. Phil. Thesis, Louisiana State University.

Dooley AC Jr. 2003. A review of the Eastern North American Squalodontidae (Mammalia: Cetacea). *Contributions from the Virginia Museum of Natural History* **11:** 1–26.

Dunn RE, Madden RH, Kohn MJ, Schmitz MD, Strömberg CAE, Carlini AA, Ré GH, Crowley J. 2013. A new chronology for middle Eocene–early Miocene South American land mammal ages. *Geological Society of America Bulletin* **125:** 539–555.

Escapa IH, Pol D. 2011. Dealing with incompleteness: new advances for the use of fossils in phylogenetic analysis. *Palaios* **26:** 121–124.

Fettuccia D de C. 2010. *Variação osteológica e desenvolvimento ontogenético das espécies do gênero Sotalia (Cetacea, Delphinidae)*. Unpublished D.Phil. Thesis, Instituto Nacional de Pesquisas da Amazonia.

Fitzgerald EMG. 2016. A late Oligocene waipatiid dolphin (Odontoceti: Waipatiidae) from Victoria, Australia. *Memoirs of Museum Victoria* **74:** 117–136.

Fleagle JG, Bown TM. 1983. New primate fossils from late Oligocene (Colhuehuapian) localities of Chubut Province, Argentina. *Folia Primatologica* **41:** 240–266.

Flynn TT. 1948. Description of *Prosqualodon davidi* Flynn, a fossil cetacean from Tasmania. *Transactions of the Zoological Society of London* **26:** 153–95.

Flynn JJ, Swisher CC. 1995. Cenozoic South American land mammal ages: correlation to global geochronologies. In: Berggren WA, Kent DV, Aubry MP, Hardenbol J, eds. *Geochronology time scales and global stratigraphic correlation*. Tulsa, Oklahoma: SEPM Society for Sedimentary Geology, 317–333.

Fordyce RE. 1981. Systematics of the odontocete whale *Agorophius pygmaeus* and the Family Agorophiidae (Mammalia: Cetacea). *Journal of Paleontology* **55:** 1028–1045.

Fordyce RE. 1994. *Waipatia maerewhenua*, new genus and new species (Waipatiidae, new family), an archaic Late Oligocene dolphin (Cetacea: Odontoceti: Platanistoidea) from New Zealand. *Proceedings of the San Diego Museum of Natural History* **29:** 147–176.

Fordyce RE. 2002. *Simocetus rayi* (Odontoceti: Simocetidae, new Family): a bizarre new archaic Oligocene dolphin from the Eastern North Pacific. *Smithsonian Contributions to Paleobiology* **93:** 185–222.

Fordyce RE, de Muizon C. 2001. Evolutionary history of cetaceans: a review. In: de Buffrenil V, Mazin JM, eds. *Secondary adaptation of tetrapods to life in water*. Munich: Pfeil Verlag, 169–233.

Fraser FC, Purves PE. 1960. Hearing in cetaceans: evolution of the accessory air sacs and structure of the outer and middle ear in recent cetaceans. *Bulletin of the British Museum (Natural History), Zoology* **7:** 1–140.

Geisler JH, Sanders AE, Luo Z-X. 2005. A new protocetid whale (Cetacea: Archaeoceti) from the Late Middle Eocene of South Carolina. *American Museum Novitates* **3480:** 1–65.

Geisler JH, McGowen MR, Yang G, Gatesy J. 2011. A supermatrix analysis of genomic, morphological, and paleontological data from crown Cetacea. *BMC Evolutionary Biology* **11:** 112.

Godfrey SJ. 2013. On the olfactory apparatus in the Miocene odontocete *Squalodon* sp. (Squalodontidae). *Comptes Rendus Palevol* **12:** 519–530.

Godfrey SJ, Uhen MD, Osborne JE, Edwards LE. 2016. A new specimen of *Agorophius pygmaeus* (Agorophiidae, Odontoceti, Cetacea) from the early Oligocene Ashley Formation of South Carolina, USA. *Journal of Paleontology* **90:** 154–169.

Goloboff PA, Carpenter JM, Arias JS, Miranda DR, Miranda-Esquivel DR. 2008. Weighting against homoplasy improves phylogenetic analysis of morphological data sets. *Cladistics* **24:** 758–773.

Goloboff PA, Catalano SA. 2016. TNT version 1.5, including a full implementation of phylogenetic morphometrics. *Cladistics* **32:** 221–238.

Goloboff PA, Torres A, Arias JS. 2017. Weighted parsimony outperforms other methods of phylogenetic inference under models appropriate for morphology. *Cladistics* 1–31. Available at: https://doi.org/10.1111/cla.12205

Gutstein CS, Cozzuol MA, Pyenson ND. 2014. The antiquity of riverine adaptations in Iniidae (Cetacea, Odontoceti) documented by a humerus from the late Miocene of the Ituzaingó Formation, Argentina. *Anatomical Record* **297:** 1096–1102.

Howell AB. 1930. Myology of the narwhal (*Monodon monoceros*). *American Journal of Anatomy* **46:** 187–215.

Ichishima H. 2016. The ethmoid and presphenoid of cetaceans. *Journal of Morphology* **277:** 1661–1674.

Kellogg R. 1923. Description of two squalodonts recently discovered in the Calvert Cliffs, Maryland; and notes on the shark-toothed cetaceans. *Proceedings of the United States National Museum* **62:** 1–69.

Kellogg R. 1924. A fossil porpoise from the Calvert Formation of Maryland. *Proceedings of the United States National Museum* **63:** 1–14.

Kellogg R. 1928. The history of whales. Their adaptation to life in the water. *The Quarterly Review of Biology* **3:** 29–76.

Kellogg R. 1959. Description of the skull of *Pomatodelphis inaequalis* Allen. *Bulletin of the Museum of Comparative Zoology* **121:** 2–26.

Keyes IW. 1973. Early Oligocene squalodont cetacean from Oamaru, New Zealand. *New Zealand Journal of Marine and Freshwater Research* **7:** 381–390.

Kimura T, Barnes LG. 2016. New Miocene fossil Allodelphinidae (Cetacea, Odontoceti, Platanistoidea) from the North Pacific Ocean. *Bulletin of the Gunma Museum of Natural History* **20:** 1–58.

Kimura T, Hasegawa Y, Okumura Y. 2009. Early Miocene platanistoid from the Mizunami Group, Central Japan. *Paleontological Research* **13:** 167–171.

Lambert O, Bianucci G, Urbina M. 2014. *Huaridelphis raimondii*, a new early Miocene Squalodelphinidae (Cetacea, Odontoceti) from the Chilcatay Formation, Peru. *Journal of Vertebrate Paleontology* **34:** 987–1004.

Lambert O, de Muizon C, Malinverno E, Di Celma C, Urbina M, Bianucci G. 2018. A new odontocete (toothed cetacean) from the Early Miocene of Peru expands the morphological disparity of extinct heterodont dolphins. *Journal of Systematic Palaeontology* **16:** 981–1016.

Loch C, Simões-Lopes PC. 2013. Dental wear in dolphins (Cetacea: Delphinidae) from southern Brazil. *Archives of Oral Biology* **58:** 134–141.

Lydekker R. 1894. Contributions to a knowledge of the fossil vertebrates of Argentina. Part II. Cetacean skulls from Patagonia. *Anales Del Museo de La Plata* **2:** 1–15.

Maddison WP, Maddison DR. 2011. *Mesquite*: *a modular system for evolutionary analysis, version 2.75*. Available at: http://mesquiteproject.org

Mead JG, Fordyce RE. 2009. The therian skull: a lexicon with emphasis on the odontocetes. *Smithsonian Contributions to Zoology* **627:** 1–248.

Mendía JE, Bayarsky A. 1981. Estratigrafía del Terciario en el Valle inferior del Río Chubut. *Abstract book of the 8vo Congreso Geológico Argentino* **3:** 593–606.

Moreno FP. 1892. Lijeros apuntes sobre dos géneros de cetáceos fósiles de la República Argentina. *Revista Del Museo de La Plata* **3:** 393–400.

de Muizon C. 1987. The affinities of *Notocetus vanbenedeni*, an early Miocene platanistoid (Cetacea, Mammalia) from Patagonia, southern Argentina. *American Museum Novitates* **2904:** 1–27.

de Muizon C. 1991. A new Ziphiidae (Cetacea) from the Early Miocene of Washington State (USA) and phylogenetic analysis of the major groups of odontocetes. *Bulletin du Muséum national d'Histoire naturelle* **4:** 279–326.

de Muizon C. 1994. Are the squalodonts related to the platanistoids? *Proceedings of San Diego Society of Natural History* **29:** 135–146.

Ness AR. 1967. A measure of asymmetry of the skulls of odontocete whales. *Journal of Zoology* **153:** 209–221.

Noriega JI, Cione AL, Aceñaloza FG. 2007. Shark tooth marks on Miocene balaenopterid cetacean bones from Argentina. *Neues Jahrbuch für Geologie und Paläontologie Abhandlungen* **245:** 185–192.

Palazzesi L, Barreda V, Scasso RA. 2006. Early Miocene spore and pollen record of the Gaiman Formation (Northeastern Patagonia, Argentina): correlations and paleoenvironment implications. *Abstract book of the 4to Congreso Latinoamericano de Sedimentología and 11va Reunión Argentina de Sedimentología* **1:** 161.

Parras A, Dix GR, Griffin M. 2012. Sr-isotope chronostratigraphy of Paleogene–Neogene marine deposits: Austral Basin, southern Patagonia (Argentina). *Journal of South American Earth Sciences* **37:** 122–135.

Perrin WF. 1975. Variation of spotted and spinner porpoise (genus *Stenella*) in the eastern Pacific and Hawaii. *Bulletin of the Scripps Institution of Oceanography* **21:** 1–206.

Perrin WF, Würsig B, Thewissen JGM. 2008. *Encyclopedia of marine mammals*, *2nd edn*. New York: Academic Press.

Pol D, Escapa IH. 2009. Unstable taxa in cladistic analysis: identification and the assessment of relevant characters. *Cladistics* **25:** 515–527.

Puttick MN, O'Reilly JE, Tanner AR, Fleming JF, Clark J, Holloway L, Lozano-Fernandez J, Parry LA, Tarver JE, Pisani D, Donoghue PCJ. 2017. Uncertain-tree: discriminating among competing approaches to the phylogenetic analysis of phenotype data. *Proceedings of the Royal Society B: Biological Sciences* **284:** 20162290.

Pyenson N, Sponberg S. 2011. Reconstructing body size in extinct crown Cetacea (Neoceti) using allometry, phylogenetic methods and tests from the fossil record. *Journal of Mammalian Evolution* **18:** 269–288.

Rommel SA. 1990. Osteology of the bottlenose dolphin. In: Leatherwood S, Reeves RR, eds. *The bottlenose dolphin*. San Diego: Academic Press, 29–49.

Rommel SA, Reynolds JE. 2008. Skeleton, postcranial. In: Perrin WF, Würsig B, Thewissen JGM, eds. *Encyclopedia of marine mammals*, *2nd edn*. New York: Academic Press, 1021–1033.

Rothausen K. 1968. Die systematische Stellung der europaischen Squalodontidae (Odontoceti: Mamm.). *Paläontologische Zeitschrift* **42:** 83–104.

Scasso R, Bellosi E. 2004. Cenozoic continental and marine trace fossils at the Bryn Gwyn Paleontological Park, Chubut. Bryn Gwyn Guidebook. *Abstract book of the 1st International Congress on Ichnology* **1:** 18.

Scasso RA, Castro LN. 1999. Cenozoic phosphatic deposits in North Patagonia, Argentina: phosphogenesis,

sequence-stratigraphy and paleoceanography. *Journal of South American Earth Sciences* **12:** 471–487.

Schulte HVW, Smith MDF. 1918. The external characters, skeletal muscles, and peripheral nerves of *Kogia breviceps* (Blainville). *Bulletin of the American Museum of Natural History* **38:** 7–72.

Simpson GG. 1935. Early and middle tertiary geology of the Gaiman Region, Chubut, Argentina. *America Museum Novitates* **775:** 1–29.

Simpson GG. 1945. The principles of classification and a classification of mammals. *Bulletin of the American Museum of Natural History* **85:** 1–350.

Slater GJ, Price SA, Santini F, Alfaro ME. 2010. Diversity versus disparity and the radiation of modern cetaceans. *Proceedings of the Royal Society B: Biological Sciences* **277:** 3097–3104.

Smith GJ, Browne KW, Gaskin DE. 1976. Functional myology of the harbour porpoise, *Phocoena phocoena* (L.). *Canadian Journal of Zoology* **54:** 716–729.

Strickler TL. 1978. Myology of the shoulder of *Pontoporia blainvillei*, including a review of the literature on shoulder morphology in the Cetacea. *The American Journal of Anatomy* **152:** 419–431.

Tanaka Y, Fordyce RE. 2014. Fossil dolphin *Otekaikea marplesi* (latest Oligocene, New Zealand) expands the morphological and taxonomic diversity of Oligocene cetaceans. *PLoS One* **9:** e107972.

Tanaka Y, Fordyce RE. 2015a. A new Oligo-Miocene dolphin from New Zealand: *Otekaikea huata* expands diversity of the early Platanistoidea. *Palaeontologia Electronica* **18:** 1–71.

Tanaka Y, Fordyce RE. 2015b. Historically significant late Oligocene dolphin *Microcetus hectori* Benham 1935: a new species of *Waipatia* (Platanistoidea). *Journal of the Royal Society of New Zealand* **45:** 135–150.

Tanaka Y, Fordyce RE. 2016. *Papahu*-like fossil dolphin from Kaikoura, New Zealand, helps to fill the Early Miocene gap in the history of Odontoceti. *New Zealand Journal of Geology and Geophysics* **59:** 551–567.

Tanaka Y, Fordyce RE. 2017. *Awamokoa tokarahi*, a new basal dolphin in the Platanistoidea (late Oligocene, New Zealand). *Journal of Systematic Palaeontology* **15:** 365–386.

Tsai C-H, Fordyce RE. 2016. Archaic baleen whale from the Kokoamu Greensand: earbones distinguish a new late Oligocene mysticete (Cetacea: Mysticeti) from New Zealand. *Journal of the Royal Society of New Zealand* **46:** 117–138.

Velez-Juarbe J, Domning DP, Pyenson ND. 2012. Iterative evolution of sympatric seacow (Dugongidae, Sirenia) assemblages during the past ~26 million years. *PLoS One* **7:** e31294.

Viglino M, Buono MR, Gutstein CS, Cozzuol MA, Cuitiño JI. 2018. A new dolphin from the early Miocene of Patagonia, Argentina: insights into the evolution of Platanistoidea in the Southern Hemisphere. *Acta Palaeontologica Polonica*. **63:** 261–277.

Woodward G, Ebenman B, Emmerson M, Montoya JM, Olesen JM, Valido A, Warren PH. 2005. Body size in ecological networks. *Trends in Ecology & Evolution* **20:** 402–409.

SUPPORTING INFORMATION

Additional Supporting Information may be found in the online version of this article at the publisher's web-site:

Appendix S1. List of specimens revised and literature used during the phylogenetic and anatomical study of the present contribution. These include additional or alternative material to those listed by Tanaka & Fordyce (2016). Specimens are held in public scientific collections.

Appendix S2. List of morphological characters used in the phylogenetic analysis, based on Tanaka & Fordyce (2016).

Appendix S3. Morphological matrix used in the phylogenetic analysis of *Phoberodon arctirostris*.

Appendix S4. Supplemental full trees of the phylogenetic analysis of *Phoberodon arctirostris*.

Appendix S5. Supplemental figures for the modern description of *Phoberodon arctirostris*.

Appendix S6. Measurements of vertebrae of all studied specimens of *Phoberodon arctirostris* (in millimetres).